



**HAL**  
open science

# Meso-structure-based thermomechanical modelling of thermoplastic-based laminates subjected to combined mechanical loading and severe thermal gradients

Yann Carpier, Benoît Vieille, Fabrice Barbe, Alexis Coppalle

## ► To cite this version:

Yann Carpier, Benoît Vieille, Fabrice Barbe, Alexis Coppalle. Meso-structure-based thermomechanical modelling of thermoplastic-based laminates subjected to combined mechanical loading and severe thermal gradients. *Composites Part A: Applied Science and Manufacturing*, 2022, 162, pp.107165. 10.1016/j.compositesa.2022.107165 . hal-03767506

**HAL Id: hal-03767506**

**<https://hal.science/hal-03767506>**

Submitted on 2 Sep 2022

**HAL** is a multi-disciplinary open access archive for the deposit and dissemination of scientific research documents, whether they are published or not. The documents may come from teaching and research institutions in France or abroad, or from public or private research centers.

L'archive ouverte pluridisciplinaire **HAL**, est destinée au dépôt et à la diffusion de documents scientifiques de niveau recherche, publiés ou non, émanant des établissements d'enseignement et de recherche français ou étrangers, des laboratoires publics ou privés.

**Meso-structure-based thermomechanical modelling of thermoplastic-based laminates subjected to combined mechanical loading and severe thermal gradients**

Yann Carpier<sup>1</sup>, Benoit Vieille<sup>1</sup>, Fabrice Barbe<sup>1</sup>, Alexis Coppalle<sup>2</sup>

1 : INSA Rouen, Normandie Univ, CNRS, Groupe de Physique des Matériaux

Avenue de l'Université, 76800 Saint Etienne du Rouvray

2 : INSA Rouen, Normandie Univ, CNRS, CORIA

Avenue de l'Université, 76800 Saint Etienne du Rouvray

e-mail : [benoit.vieille@insa-rouen.fr](mailto:benoit.vieille@insa-rouen.fr)

**Abstract**

This paper presents a numerical modelling methodology to investigate the thermo-mechanics of carbon reinforced thermoplastic-based laminates in the situation of mechanical loading combined to thermal gradients. It concerns in particular the case of thermal irradiation on one face of the laminate, where temperature varies both from point to point of the laminate and through time, and ranges from the ambient to the temperature of matrix decomposition onset. Temperature is the key variable to determine the physical state and the properties of each phase of the composite. Particular attention is therefore paid to identifying the respective material properties according to temperature. The developed numerical model is based on an explicit representation of the yarn-matrix spatial arrangement within a representative volume element of the considered laminate. From this model the influence of the heterogeneous matrix thermal degradation on the macro-scale thermal dependent properties of the composite is discussed. Such a modelling requires the consideration of a wide range of phenomena (modification of physical and mechanical properties) and a comprehensive set of thermal boundary conditions (heterogeneous distribution of heat flux density on the sample surface, convection, radiation). The proposed model provides a very good prediction of the laminate's stiffness evolution according to temperature up to the onset of thermal decomposition temperature. It further enables to analyze the gradual efforts take up between the plies when a constant mechanical loading is combined to a heat exposure.

**Keywords:** thermal-mechanical coupling, thermoplastic, carbon fibers, modelling, identification

**Nomenclature**

<b>Variables</b>		$t$	Time
$T$	Temperature	$\epsilon$	Strain
$q$	Heat flux	$\sigma$	Stress
<b>Parameters</b>		<b>Subscripts</b>	
$\rho$	Volume density	$bf$	Back face of the exposed plate
$c$	Specific heat capacity	$\Phi$	Constituent ( $\Phi = cp, m, fb$ )
$\lambda$	Thermal conductivity	$cp$	Composite plate (macroscale)
$a(T_1 \rightarrow T_2)$	Coefficient of variation of $\lambda$ between $T_1$ and $T_2$	$m$	Matrix
$h$	Convective heat transfer coefficient	$fb$	Fiber bundle (yarn)
$\epsilon$	Emissivity	<b>Superscript</b>	
$\theta$	Absorptivity	$s$	
$V$	Volume fraction	$p$	Planar (macroscale plate)

$H$	Hooke tensor	$z$	Through-the-thickness (macroscale plate)
$E$	Young's modulus or stiffness	$\alpha x$	Axial (mesoscale fiber bundle)
$\nu$	Poisson's ratio	$r$	Radial (mesoscale fiber bundle)
$\alpha$	Thermal dilation coefficient	$L$	Longitudinal (macroscale plate)

## 1 Introduction

Under critical service conditions (such as an aircraft engine fire), aeronautical structural parts made of polymer matrix composite materials can be subjected to simultaneous heat flux and mechanical load. Research on the fire performance of composite materials began at the end of the 1970s, in parallel with their development for aerospace applications. As composite parts were starting to be integrated in positions where their role was also to shield against heat, the emphasis was then focused on analyzing their integrity under the exposure of intense thermal stress. In the mid-1990s, the first studies on the mechanical strength of a composite material subjected to both mechanical loading and thermal stress (more or less representative of fire conditions) were published [1]. Most publications dealing with the fire behavior of polymer matrix composites are related to thermosetting matrices [1-11], which have been used for almost 40 years in these sectors (carbon/epoxy, carbon/phenolic, glass/vinylester or glass/polyester). From the end of the 1990s, the use of thermoplastic matrix composite materials has been developed in many industries. The motivations are numerous: easier implementation, higher production rates, environmental regulations and better fire-performance. However, their thermomechanical behavior has been far less studied than the one of thermosetting-based composites (TSCs) and this has hindered their development for structural applications [3-12]. Even though they display interesting mechanical properties, TSCs also present undeniable drawbacks, such as the need for low-temperature storage, a hard-to-control cure process, a very long curing process, and handmade draping, which causes most of the irreversible defects of the manufacturing process. High-performance thermoplastic resins (e.g. PEEK and PPS) offer a promising alternative to TS resins. Indeed, the material consolidation does not involve exothermic curing reactions, resulting in shorter autoclave cycle times, although the temperatures involved are generally higher than those for TSCs. The meltability of thermoplastics is also an advantage for recycling purposes.

### Thermomechanical coupling in C/PPS laminates

PolyPhenylene Sulfide thermoplastic polymer (PPS) is a good candidate for applications in aeronautics. It is a semi-crystalline polymer and it is thus strain-rate or cooling rate sensitive. The glass transition temperature of PPS is typically  $T_g = 98^\circ\text{C}$  and its melting temperature  $T_m = 280^\circ\text{C}$  [13]. The degree of crystallinity of PPS matrix is close to 30% and the initial porosity ratio is very small (less than 2%). To better understand the concomitant changes in the thermal and mechanical behaviors of PPS-based composites under fire exposure, the first step classically consists in investigating the influence of temperature under isothermal conditions [13,14], before extending to the case of heterogeneous temperature fields [15-19]. A specificity in [16-18] was to combine the thermal aggression to the mechanical loading (in tension or compression) and to make simultaneous measurements of temperatures and mechanical response through time, up to temperatures above the onset of polymer matrix decomposition. This allowed to clearly delineating the dependencies of the laminates mechanical behavior to the thermal conditions at play, could they be isothermal or anisothermal and transient.

In the prior analyses presented in [14], stable and homogeneous temperature conditions were applied by means of a tube furnace composed of 3 heating zones and positioned between the grips of the mechanical testing machine. From the tensile tests which were carried out on quasi-isotropic carbon fibers reinforced PPS at temperatures ranging from ambient to 520°C, it appeared that the retention of the laminate's longitudinal stiffness remains relatively high (about 70% of its initial value) beyond the temperature of polymer decomposition onset. At the same time, the ultimate strength dramatically decreases (about 25% of its initial value). The obtained results show that matrix transformations are instrumental to rule the tensile behavior of quasi-isotropic C/PPS laminates. Matrix melting significantly influences the damage mechanisms within the laminate and matrix onset decomposition leads to porosities growth within the laminates, ultimately contributing to the degradation of the mechanical properties.

In the extension of the analyses to heterogeneous and transient thermal conditions, the purpose was to analyze the temperature distribution and the related thermal decomposition phenomena within a plate of laminates exposed to a medium-intensity heat flux (typically 50kW/m<sup>2</sup>) [16-18]. Such heat fluxes lead to significant thermal gradients within composite structures, leading to (i) a gradient in both thermal and mechanical properties, (ii) a gradient of chemical composition and (iii) thermally induced damages. By comparing the temperature profiles on both exposed and back surfaces of C/PPS laminates subjected to a 50kW/m<sup>2</sup> heat flux, the through-the-thickness temperature gradient has been shown to be significant (about 320°C in the steady state). As the onset of decomposition temperature is reached on the exposed surface but not on the back surface, a consequential gradient of the chemical composition is also obtained through the thickness. For heat fluxes ranging from 20 to 50kW/m<sup>2</sup>, a prior fire exposure is highly detrimental to the compressive mechanical properties as the residual strength and stiffness decrease by 75% and 55%, respectively. Ultimately, the contribution of laminates' plies to bear the mechanical load is directly correlated to their decomposition state, adversely affecting their structural capabilities in terms of strength and stiffness.

### **Modelling of thermomechanical coupling in polymer-matrix composites**

Over the past twenty years, many models have been developed to account for the coupling of thermal and mechanical phenomena within composite materials [20-27], with a particular attention paid to fire modelling [28-46]. In the early eighties, Pering *et al.* have developed an analytical model to account for the degradation of tensile and shear properties of a composite exposed to fire or high temperature [31]. Similarly, Chen *et al.* have simulated the failure of carbon/epoxy laminates subjected to combined thermal and mechanical loading [32]. This model is based on the prediction of the through-the-thickness temperature obtained by using a one-dimensional finite difference code. The effects of ablation, degradation of thermo-physical properties at elevated temperatures, and radiation and convective heat losses are included in the formulation as well as the temperature-dependency of mechanical properties. Considering a similar approach, Griffis *et al.* have developed an analytical procedure for predicting the loss in integrity of composite structures subjected to simultaneous intense heating and applied mechanical loads [33]. These authors have considered a nonlinear two-dimensional finite difference thermal analysis associated with a mechanical model based on the Mindlin theory coupled to a maximum stress failure criterion. In 1995, Gibson *et al.* proposed a 1D thermal model considering the three main thermal phenomena which occur in a composite material exposed to fire (through-the-thickness conduction, matrix decomposition and convective mass transfer of volatiles) [34]. It has been subsequently used in many studies on

the mechanical behavior under fire exposure [35]. Feih *et al.* combined it with a modelling of the material softening to predict the time-to-failure of laminates supporting a static tensile or compressive stress during one-sided heating. To do so, the average strength of the material is calculated from the integral over the thickness of the local temperature-dependent strengths and compared to the material strength. The accuracy of the model has been tested using time-to-failure of woven E-glass/vinyl ester laminates exerting a combination of fire exposure and compression loading [29]. A few years later, the influence of carbon fiber oxidation on the tensile properties was added in the model to study the resistance of unidirectional carbon/epoxy composites exposed to fire [30]. More recently, Swanson *et al.* considered an empirical model to extrapolate and predict failure times using a stretched exponential function, based on mechanical preload heat flux, and material thickness [41]. In Bhat *et al.*, the collapse of basal fiber laminates upon compression loading combined to thermal irradiation has been studied [42]. The developed model provides the softening rate and the failure stress of the laminates by accounting for the mechanisms of global buckling and material failure. All these thermo-mechanical models are useful to estimate the failure time of loaded composite structures exposed to high temperature or fire. However, these references are limited to the thermo-mechanical macro-scale behavior of composite laminates. They do not predict the progressive stress redistribution between the plies resulting from the heterogeneous thermal degradation of the polymer matrix. They are thus not able to predict how the residual strength evolves through time in this very rapidly varying and case-sensitive situation of a fire exposure. To reach this goal, it is necessary to account for an accurate degradation of the properties through the thickness.

### **Identification**

Modelling the behavior of laminates exposed to fire requires the consideration of various phenomena. Due to the heterogeneous and anisotropic nature of these materials, the number of parameters and properties needed to achieve this is *a priori* very large. Ideally, each property (and its evolution with temperature) would be determined through dedicated experimental analyses enabling to separate the involved physical phenomena. However, this approach comes up against material constraints, especially for physico-chemical properties: each of them generally requires dedicated facilities which are not necessarily designed for such high temperature levels. Several approaches can be considered to deal with this problem. It is possible to consider fewer phenomena, by determining empirically which ones play the dominant roles on the response of the material, or through sensitivity analyses [43]. Reverse identification methods can also be used. Their objective is to find the set of parameters allowing an optimal reproduction of experimental results. In their seminal work, Lautenberger *et al.* pointed out that one of the impediments to improving thermal simulation results was the lack of methods for making appropriate use of data from standardized tests such as those performed with a cone calorimeter [44]. Using a genetic algorithm, they identified the parameters of a heat transfer and of a pyrolysis model, which enable to reproduce the front face temperature and mass loss rate measured during tests performed with a cone calorimeter. Such methods were used in several other studies dealing with fire behavior of composite materials [45]. One of the drawbacks of identification methods applied to a large number of parameters is the compensation effect between parameters. For example, if two parameters affect the thermal response in the same direction, the error on one can be compensated by changing the other, resulting in a large number of mathematically correct parameter sets, but incorrect from a physical standpoint. To deal with this, Lattimer *et al.*

studied the influence of properties on the thermal response (surface temperature during the transient phase for example) and separately identified the homogenized properties of a composite material subjected to fire [46].

### **Novelty of this study**

Previous investigations on thermally irradiated thermoplastic-based laminates [16-17] have enabled to identify the complexity of the physical interactions at play in the scenario of a fire exposure: (i) the temperature field is characterized by both high gradients and rapid evolution through time; (ii) even for reasonable incident heat fluxes and times of exposure (few tens of kW/m<sup>2</sup> and seconds), the range of encountered temperatures includes the three transitions of the polymer matrix (glass transition, melting and decomposition); (iii) the capacity of the laminate to sustain a load remains considerable along the process of polymer matrix degradation and becomes detrimental only when the polymer is fully decomposed in all its thickness.

In this context of a fire scenario, where the rate of degradation of the laminate's mechanical properties is the key controlling factor, accurate descriptions of the transient thermal transfers and of the mechanical properties temperature dependencies are two main requirements for the development of a predictive model. As the two constituents of the laminate -polymer matrix and fiber bundles- have contrasted thermal and mechanical properties, their spatial arrangement in the laminate can be inferred to play a prominent role. The novelty of this study lies in the fact that it combines all the pre-identified characteristics involved in the fire scenario: (i) an explicit representation of the meso-structure constituted by the woven fiber bundles and the polymer matrix in a representative volume element, (ii) a variation of the thermal and mechanical properties according to temperature, from the ambient to the onset of polymer matrix decomposition, where its mechanical stiffness is quasi-completely degraded.

Consequently, the developed model calls upon a considerable number of temperature dependent material parameters which need to be determined. Given the difficulty of identifying each of them one by one from pre-established and straightforward experimental analyses, an identification methodology of the thermal properties has been developed. It corresponds to the first main challenge of the study. The quality of the parameters' identification is discussed by confronting experimentally measured temperatures to simulated ones in three cases of one face heat exposure. This identification is then validated on the thermomechanical ground by comparing the simulated evolution of the plate longitudinal stiffness to the experimental one under isothermal conditions from the ambient to the onset of matrix decomposition. Then the thermomechanical model is used to study the progressive efforts take-up of the respective fiber bundles in the case of a one face thermal irradiation. The proposed model is driven by the chosen material (C/PPS laminates) and the experimental thermomechanical set-up used for the identification. However, it can be extended to any kind of carbon or glass reinforced laminates subjected to a combined heat flux and moderate mechanical load. The multiscale approach and the identification methodology will remain the same.

The manuscript is organized as follows. Section 2 defines the considered physical problem: the studied material, the hypotheses used to build the Representative Volume Element (RVE), the conditions it is exposed to, conforming to the experimental set-up, the hypotheses on the involved physics and the resulting mathematical problem to solve. Section 3 presents the different experimental means employed in this study. Section 4 provides a comprehensive description of the identification procedure. Section 5 presents firstly the validation of the

thermomechanical model for tensile isothermal conditions and secondly the multiscale analyses on the thermomechanics of the laminate under combined heat flux and mechanical loading.

## 2 Physical problem

### 2.1 Studied material

The composite material is a stacking of carbon fabric reinforced laminates consisting of a semi-crystalline high-performance PPS supplied by the Ticona company. The woven-ply prepreg, supplied by SOFICAR, consists of 5-harness satin weave carbon fiber fabrics (T300 3K 5HS) whose weight fraction is 58%. It corresponds to a volume fraction of 50%. The fabric is balanced in warp and weft directions such as each ply consists of the same mass fraction of fibres oriented at 0° (warp direction), and at 90° (weft direction). The prepreg plates are hot pressed according to a quasi-isotropic stacking sequence [(0,90)/(±45)/(0,90)/(±45)/(0,90)/(±45)/(0,90)]. The consolidated laminates were obtained from hot pressed prepreg plates according to cycles presented in [47]. The void volume fraction is very small (less than 2%) [48].

As illustrated on the cross section of Figure 1, the edge microscopic observation of these laminates shows a large number of matrix-rich regions, resulting from the non-planar inter-ply structure of woven plies. As the material is exposed to fire, it is suspected that the thermal decomposition of these plain matrix regions will play an important role on the mechanical stresses' distribution within the laminates' plies. The characteristic temperatures of the solid-state modifications within a PPS polymer are reported in Table 1 [13]. They are directly related to the transformation within the matrix since for carbon fibers, the first thermally induced transformation occurring upon heating is the oxidation and it happens at a temperature significantly higher than the range of presently studied temperatures. At this stage of the presentation, the transition temperature is given within an interval since it significantly depends on the studied PPS.

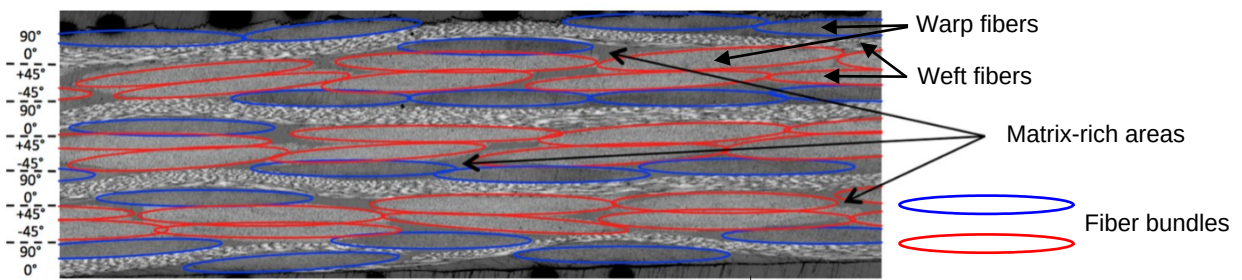


Figure 1 : Through-the-thickness optical microscopic observation of C/PPS quasi-isotropic laminates showing the carbon fiber bundles distribution in warp and weft directions (carbon fibers woven fabrics) and matrix-rich areas

Glass transition temperature $T_g$	Melting temperature $T_m$	Decomposition temperature $T_{d,0}$
90-100°C	220-295°C	450-500°C

Table 1 : Characteristic temperatures of solid-state transformations within C/PPS [13].

## 2.2 Object of study, thermal and mechanical loading

As described on Figure 2, the object of study is a finite-size plate of the considered composite. It is subjected to an in-plane mechanical load (imposed stress or strain) combined with an exposure to an incident heat flux  $q_i$  on its front face. The heat transfers on the opposite face (back face) are governed by natural convection with the surrounding air at temperature  $T_{ext}$  and radiation transfers with the environment (air and outer faces of the laminates), also at the temperature  $T_{ext}$ . On lateral faces, either adiabatic conditions ( $q=0$ ) or imposed temperature fields  $T_{imp}$  are set. The heat flux absorbed on the exposed face ( $q_{absorbed}$ ) is assumed to be proportional to the incident heat flux  $q$ , as defined in Eq. 1, where  $\theta$  is the absorptivity of the plate surface:

$$q_{absorbed} = \theta \cdot q_i \quad (1)$$

The radiation heat transfers at the back face are described by the Stefan-Boltzmann's law [49]:

$$q_{radiant} = \epsilon \cdot \kappa \cdot (T_{bf}^4 - T_{ext}^4) \quad (2)$$

$T_{bf}$  is the temperature of the back face,  $\epsilon$  is the emissivity of the composite material face and is considered to be homogeneous and  $\kappa$  is the Stefan-Boltzmann constant. Under the assumption of a grey body, absorptivity and emissivity are considered to be equal:  $\epsilon = \theta$ .

The convection heat transfers at the back face are described by Eq. 3:

$$q_{convection} = h \cdot (T_{bf} - T_{ext}) \quad (3)$$

$h$  is the coefficient of heat transfer by convection.

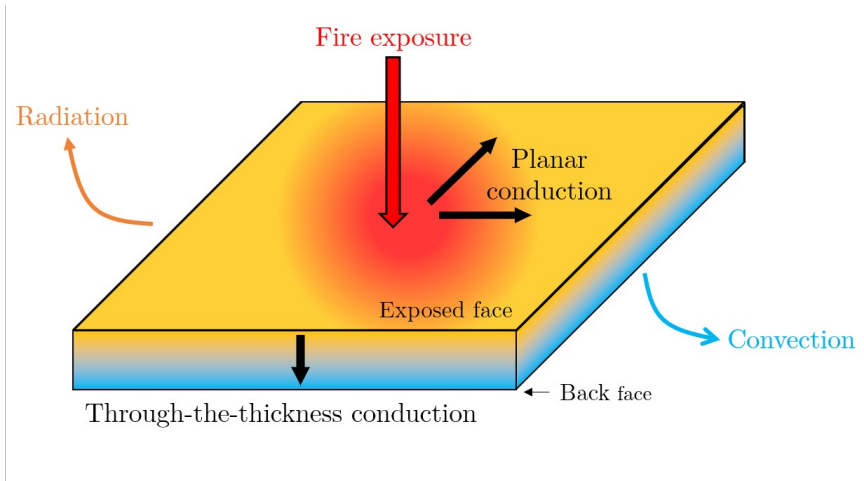


Figure 2 : Schematic of the thermal problem

## 2.3 The representative volume element and its meso-structure

The incident heat flux is of the order of few tens of kW/m<sup>2</sup> whereas the environment is typically at the ambient temperature. In this context, high thermal gradients occur, especially through the thickness of the plate. Given the range of temperatures at stake, dramatic changes are caused on the physical properties of the thermoplastic matrix whereas the carbon fibers are much less affected and remain in the same solid state. These thermally

induced changes in the physical properties of the matrix are known to affect considerably the mechanical behavior of C/PPS plates [16-18]. If, as mostly often considered in the literature, the conditions are isothermal, then the properties of the matrix are presumably uniformly distributed within the plate. It is then possible to construct macroscale elasto-visco-plastic laws with very good capabilities to reproduce the mechanical behavior of the plate up to the matrix glass transition temperature [51-53]. However, in the present case of severe three-dimensional thermal gradients with the matrix co-existing at highly contrasted states depending on its location in the plate, it is necessary to account for the actual 3D spatial arrangement of the matrix within the plate. This justifies to base the thermomechanical modelling on an explicit representation of the three-dimensional woven meso-structure over a Representative Volume Element of the plate. This RVE should at least have the thickness of the plate in order to set boundary conditions corresponding directly to those on the front and back face of the plate. The in-plane size of the RVE is that of the elementary cell of the in-plane periodic structure.

A first assumption is then made: given the small volume fraction of matrix in the fiber bundles (17%), and since fibers are unidirectional within a fiber bundle, a fiber bundle is assimilated to a homogeneous material with thermal and mechanical properties defined as those of an equivalent isotropic transverse homogeneous medium in the sense of homogenization theories.

A representation of this RVE is provided in Figure 3. Its characteristic dimensions are given in Table 2. To sum up, it consists of two homogeneous phases whose spatial arrangements reproduce the woven meso-structure of the considered laminates:

- the matrix which is considered as an isotropic material from both thermal and mechanical standpoints,
- the fiber bundles, with isotropic transverse thermal and mechanical properties which are defined locally (on the mesoscale of the RVE) according to the orientation of the fibers with respect to the global frame of the RVE.

The meso-structure of the RVE is built using the Texgen software [54]. It allows the design of any type of woven meso-structure by controlling parameters such as weaving, layering, strand dimensions and spacing, ply thickness, etc. The parameters used to model the RVE of the quasi-isotropic laminate have been determined by Daggumati *et al.* on the same material [55]).

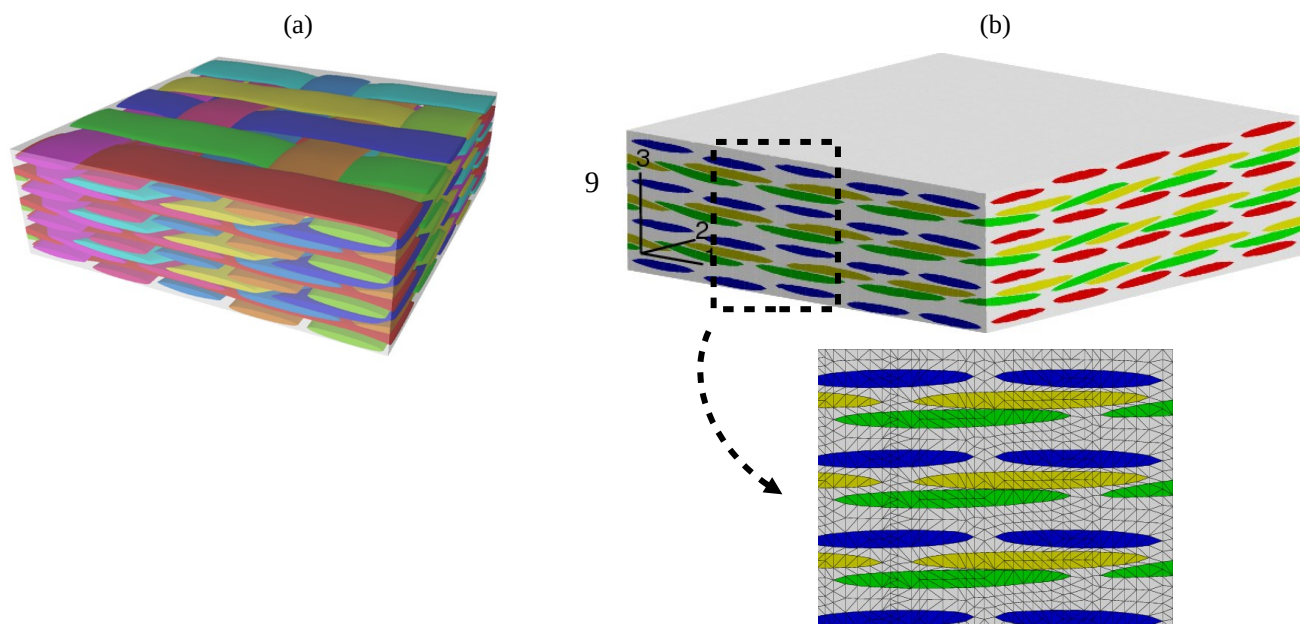


Figure 3 : Woven meso-structure of the RVE: (a) as generated with Texgen, (b) as meshed for the finite elements analyses. In the meshed RVE, each color corresponds to a fiber orientation ( $0^\circ$ ,  $90^\circ$ ,  $45^\circ$ ,  $-45^\circ$ )

Parameter	RVE sides	RVE thickness (7 plies)	Fiber bundle width	Fiber bundle thickness	Gap between fiber bundles
Dimensions (mm)	7.4 x 7.4	2.18	1.31	0.162	1.46

Table 2 : Characteristic dimensions of the woven meso-structure in the RVE

By definition, spatial averages over the whole RVE provide the effective properties of the Homogeneous Medium it is Equivalent to (HEM), i.e. the macroscopic properties of the composite material seen as a homogeneous material. Alternative uses of the RVE thermal effective properties and of a macroscale thermal modelling of the composite plate will be made in the process of identification of the thermal parameters. In accordance with the description of the composite woven meso-structure, and given the strong isotropic transverse character of thermal conduction in fibers, the thermal conduction of the plate is itself isotropic transverse on the macroscale. Other thermal properties are isotropic. With a similar reasoning, the macroscale mechanical properties of the plate can be considered to be isotropic transverse. The finite element method is used for solving the thermomechanical problems on both scales. To this purpose, the RVE is discretized into an unstructured mesh of 2351777 4-node-tetrahedral elements. The macroscale homogeneous composite plate is meshed into 180000 8-node-hexahedral elements with full integration. Simulations are performed with the software package Z-set [56].

#### 2.4 Weak thermo-mechanical coupling hypothesis

A priori, all the physical properties (solid-state, thermal and mechanical) of the RVE constituents are dependent on temperature. The main challenge of the modelling is precisely to have an accurate description of this temperature dependence for each material parameter. As classically done for thermo-mechanical problems with quasi-static medium range mechanical loads, we assume that the temperature at a point affects its mechanical state (thermal dilation) but there is no reciprocal effect. This corresponds to the hypothesis of a weak coupling between heat transfers and mechanics. It allows the thermal modelling and the mechanical modelling to be chained at each time increment  $\Delta t$  of the simulation according to two successive steps: given the temperature field  $T(t)$  at the instant  $t$ ,

1. the thermal state at  $(t + \Delta t)$  is determined, accounting for the updated thermal parameters at  $(t + \Delta t)$ ,
2. the mechanical state at  $(t + \Delta t)$  is deduced from the temperature field  $T(t + \Delta t)$  and from the mechanical boundary conditions, accounting for the mechanical parameters updated at  $(t + \Delta t)$ .

#### 2.5 Macro-scale and meso-scale thermal modelling

The identification procedure of thermal properties relies on two scales of simulation:

- the macroscale of the considered plate, where the composite is considered as a homogeneous isotropic transverse material,
- the meso-scale as described in the RVE.

At both scales, first the heat conservation equation is solved, then the mechanical balance equation. Let us note  $\Phi$  the index defining the considered homogeneous phase:  $\Phi = cp, m, fb$  respectively for the composite plate on the macroscale, the matrix and a fiber bundle.

Taking the Fourier law to describe the relation between temperature and heat flux, the heat conservation equation for the constituent  $\Phi$  reads:

$$\rho_{\Phi} \cdot c_{\Phi} \cdot \frac{\partial T}{\partial t} = \nabla \cdot (\lambda_{\Phi} \nabla T) \quad (3)$$

where  $\rho_{\Phi}$  is the volume density,  $c_{\Phi}$  is the specific thermal capacity,  $\lambda_{\Phi}$  is the conductivity and all of them a priori depend on temperature.

All properties are isotropic except the conductivities of the plate and of the fiber bundles. Hence all parameters are scalars except  $\lambda_{cp}$  and  $\lambda_{fb}$ . As described in Eq. 4, they are second-order tensors.  $\lambda_{cp}$  is defined in the global plate framework represented on Figure 3b. The indexes  $p$  and  $z$  refer to the in-plane and out-of-plane directions respectively.  $\lambda_{fb}$  is defined in the local framework of a fiber bundle (common to the global framework for  $0^{\circ}$  oriented fibers). The indexes  $ax$  and  $r$  refer to the axial and radial directions respectively.

$$\lambda_{cp} = \begin{bmatrix} \lambda_c^p & 0 & 0 \\ 0 & \lambda_c^p & 0 \\ 0 & 0 & \lambda_c^z \end{bmatrix} \quad \lambda_{fb} = \begin{bmatrix} \lambda_{fb}^{ax} & 0 & 0 \\ 0 & \lambda_{fb}^r & 0 \\ 0 & 0 & \lambda_{fb}^r \end{bmatrix} \quad (4)$$

## 2.6 Meso-scale mechanical modelling

The motivations of this study are to establish the potential of a meso-structure-based approach to describe the thermo-mechanics of composite laminates in the presence of severe thermal gradients on a large range of temperature. As a first stage of the development of such a complex approach, where it has been shown experimentally that thermally induced degradation of the matrix was playing a prominent role, only moderate mechanical loads are under concern and all constituents are considered to have a linear elastic behavior, *a priori* all depending on temperature. This elasticity is isotropic for the matrix, described by the Young's modulus  $E_m$  and the Poisson's ratio  $\nu_m$ . It is isotropic transverse for fiber bundles, described by the Hooke tensors  $H_{fb}$ . Notations for the macroscale elasticity and thermal dilation do not need to be defined in the present study. Thermal strain is supposed to be isotropic for all constituents and is thereby characterized by their respective thermal dilation coefficients  $\alpha$ .

## 2.7 Summary of the physical parameters

Table 3 provides a summary of all the physical parameters involved in the thermomechanical problem at both the macroscale of the composite plate and the mesoscale of the RVE. The coefficient of convection heat transfer and the emissivity correspond to wall transfer coefficients, which are not only dependent on the material thermomechanical properties but also other surface properties. They are supposed to be uniform and independent on temperature. Other parameters are material parameters and are supposedly dependent on temperature.

Physical property	Composite plate (macroscale)	Fiber bundles (mesoscale)	Matrix (mesoscale)
Convection heat transfer		$h$	
Emissivity (and absorptivity)		$\varepsilon$	
Volume density	$\rho_{cp}$	$\rho_{fb}$	$\rho_m$
Specific heat capacity	$c_{cp}$	$c_{fb}$	$c_m$
Thermal conductivity	$\lambda_{cp}^p, \lambda_{cp}^z$	$\lambda_{fb}^{ax}, \lambda_{fb}^r$	$\lambda_m$
Elasticity: Hooke tensor or (Young's modulus, Poisson's ratio)		$L_{fb}$	$E_m, \nu_m$
Thermal dilation	10	$\alpha_{fb}$	$\alpha_m$

Table 3 : Physical parameters of the thermomechanical problem on the composite plate macroscale and the RVE mesoscale

### 3 Experimental analyses means

This section presents the different experimental means employed for the determination of thermal and mechanical parameters. It concerns both the devices which directly provide measures of the thermal parameters and the thermomechanical set-ups originally adapted for the tackled problem.

#### 3.1 Differential Scanning Calorimetry

Differential Scanning Calorimetry (DSC) is used to measure the specific heat capacities of the composite and of its constituents. The methodology and the results are presented in section 4.2. Measurements have been performed at modulated temperature using a DSC Q2000 (TA instruments) machine. Samples of about 10 mg were encapsulated in aluminum capsules. The specific heat capacity has been calibrated using sapphire as a reference. A "heat only" protocol was chosen using the following parameters: heating rate of  $\beta_h = 2 \text{ K.min}^{-1}$ , amplitude  $A_T = 0.32 \text{ K}$  and an oscillated period of  $T = 60 \text{ s}$ . The testing temperature ranges from  $20^\circ\text{C}$  to  $300^\circ\text{C}$  (maximum temperature allowed by the device).

#### 3.2 Dynamical Mechanical Analysis

The temperature-dependence of the matrix elastic behavior (provided by the storage modulus) have been characterized with rectangular specimens ( $35 \times 12 \times 2 \text{ mm}$ ) in bending mode using a DMA Q800 (TA Instruments) machine. Testing temperature ranges from  $28^\circ\text{C}$  to  $200^\circ\text{C}$  at a heating rate of  $2 \text{ K.min}^{-1}$  with an amplitude of  $15 \mu\text{m}$  and a frequency of  $1\text{Hz}$ .

#### 3.3 Thermal conductivity measurement

The out-of-plane thermal conductivities of PPS and C/PPS plates have been measured using the guarded hot plate method. The principle consists in reproducing in a finite size system the steady-state heat transfer in an infinite plate between two isothermal planes, one warm and the other cold. To do so, a heat flux produced by Joule effect at the hot plate diffuses in equal parts into the thickness of the samples to be characterized, which are each in contact with a cold plate. Assuming unidirectional heat transfer in the normal plate direction (infinite plate hypothesis), the thermal conductivity of the sample is calculated from the variation of temperature across

the thickness. The samples dimensions were 40x40mm<sup>2</sup> and the measurement zone was a 25-millimeter diameter disc. The measurements have been realized at the ambient temperature on 4 samples (C/PPS and PPS).

### 3.4 Heat flux irradiation bench

An experimental bench has been specifically designed for applying a thermal aggression on one face of a composite plate combined with a mechanical loading [16-17]. The incident heat flux is provided by an electrical radiant heat source integrated within the so-called cone calorimeter (Figure 4). The power in the electrical resistance is controlled by a dedicated device, which enables to accurately set the heat flux density. Three heat fluxes (30-40-50 kW/m<sup>2</sup>) have been considered in order<sup>11</sup> to sweep across a wide temperature range through the laminate's thickness (200-600°C). This bench has been used in previous works [16-17] to characterize the thermo-mechanical behavior of carbon PPS quasi-isotropic plates exposed to a simultaneous heat flux and a compressive or tensile load. In the present study, it is only used for the identification of thermal properties.

13

The specimens are plates of 100x150 mm<sup>2</sup>, as for the compression tests in [17]. This geometry has been preferred to the one used for tensile tests ([16]) because of its larger surface: significant in-plane temperature gradients can then be obtained on the back face, thereby providing reference data which can be harnessed for both through-the-thickness and in-plane thermal properties identification. As in our previous analyses, a normalized anti-buckling fixture has been used to fix the plates in the experimental set-up.

A comprehensive set of thermal time-continuous measurements is collected for each test. It is required both for the thermal boundary conditions of the simulations and to constitute the reference data of the identification procedure:

- (i) The incident heat flux on the front face of a specimen is preliminarily determined from measures by means of a Gardon gauge on a plate with 24-holes, specifically designed for this purpose. This measured heat flux is directly used as a boundary condition in the simulations.
- (ii) The temperature field on the back face of a specimen is measured by means of infrared thermography (with a rear mirror). A Thermacam camera PM 575 manufactured by FLIR Systems has been used. The value of emissivity was set at 0.90, as most frequently set for composite materials with carbon fibers (see e.g. [31]). The back-face temperature fields constitute the main part of the reference data for the identification and for the validation of the identification.
- (iii) The temperature on the front face is measured at different points by means of type K thermocouples. A reliable temperature measurement from infrared thermography is indeed virtually impossible to perform on the front face because of the cone-calorimeter occultation. Yet, were it possible, the obtained measures would be questionable because of the numerous sources of errors related to the environment: hot atmosphere, gas pyrolysis, reflection of a part of the radiation on the surface of the sample. This set of front-face temperature measurements completes the reference data for the identification.
- (iv) The temperatures on the edges of a specimen are measured at different points by means of type K thermocouples. This set of temperature measurements is used as conductive thermal boundary conditions in the simulations.

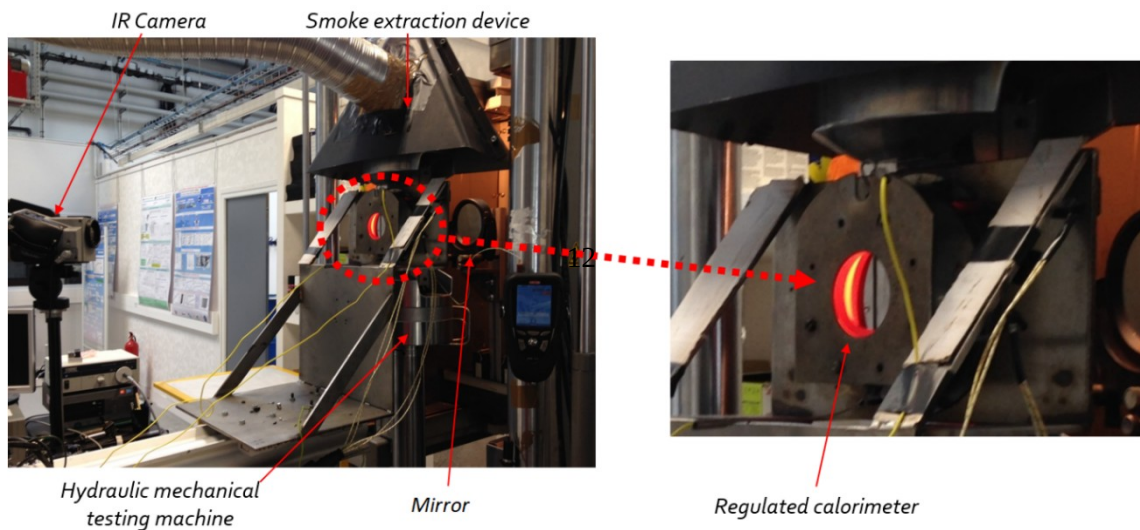


Figure 4 : Experimental set-up allowing the simultaneous following operations: front-face controlled incident heat flux (cone calorimeter), back—face temperature field measurement (infrared thermography), localized temperature measurement on the front and lateral faces (thermocouples)

### 3.5 Isothermal tensile tests

An MTS electromechanical machine with a load capacity of 100 kN is used to determine the stiffness of the composite plate at different temperatures from the ambient to the temperature of matrix decomposition  $T_{d,0}$ .

It is equipped with a three-zone tube furnace, which enables to expose the specimen to a homogeneous and stable temperature over the full range of temperatures of interest in the present study. Because of the dimensions of the furnace and in order to prevent any thermal damage on the grips of the tensile machine, specific dog bone specimens are required. Their overall length is 295mm and the gauge length is 200 mm. A dedicated high temperature extensometer can be adapted to measure the strain in the gauge region. In accordance with the European standards EN 6035 [57], the elastic longitudinal (in-plane) modulus of the composite plate is determined from the variation of the force between two prescribed axial strains (0.025% and 0.05%). Details on this set-up and on the high temperature tensile properties of C/PPS can be found in [15].

## 4 Thermal modelling

### 4.1 Preliminary statements on thermal parameters and their temperature dependence

The following assumptions are made concerning the dependence of thermal parameters to temperature:

- The densities of the constituents, the emissivity and the convection coefficients are independent on temperature; this assumption is reasonable as long as the material is a continuous medium without voids, i.e. as long as the material is not decomposed,

- The axial conductivity of fiber bundles  $\lambda_{fb}^{ax}$  changes linearly within the temperature range  $[T_0, T_{d,0}]$ ; this is consistent with the observation made on carbon fibers at higher temperatures [58-59],
- The radial conductivity of fiber bundles  $\lambda_{fb}^{rad}$  and the conductivity of the matrix  $\lambda_m$  vary linearly according to temperature within the successive temperature intervals corresponding to the characteristic solid-states of the matrix:  $[T_0, T_g], [T_g, T_m], [T_m, T_{d,0}]$
- As a consequence, the conductivity of the composite plate through the thickness ( $\lambda_{cp}^z(T)$ ) will also vary linearly within each aforementioned temperature interval,
- The in-plane conductivity of the composite plate ( $\lambda_{cp}^p(T)$ ) is assumed to be governed prominently by the axial conductivity of the fibers since the out-of-plane crimp regions of the fiber bundles represent a very small volume fraction of the plate and since the axial conductivity of the fibers is much larger than that of the matrix. As a consequence,  $\lambda_{cp}^p(T)$  is assumed to vary linearly within the temperature range  $[T_0, T_{d,0}]$ .

Let us note  $a_\Phi(T_1, T_2)$  the coefficient of variation of the thermal conductivity of the phase  $\Phi$  within the interval  $[T_1, T_2]$ . The conductivity of the phase  $\Phi$  at temperature  $T$  can then be written:

$$\lambda_\Phi(T) = \lambda_\Phi(T_1) + a_\Phi(T_1, T_2) \cdot (T_2 - T) \quad \forall T \in [T_1, T_2] \quad (7)$$

Given this previously set assumptions, there are 16 parameters involved in the mesoscale thermal modelling over the range  $[T_0, T_{d,0}]$ . They are listed in Table 4.

Physical property	Fiber bundles	Matrix
Volume density	$\rho_{fb}$	$\rho_m$
Specific heat capacity	$c_{fb}(T)$	$c_m(T)$
Thermal conductivity at $T_0$	$\lambda_{fb}^{ax}(T_0), \lambda_{fb}^r(T_0)$	$\lambda_m(T_0)$
Coefficients of thermal conductivity variation	$a_{fb}^{ax}(T_0, T_{d,0})$ $a_{fb}^r(T_0, T_g), a_{fb}^r(T_g, T_m), a_{fb}^r(T_m, T_{d,0})$	$a_m(T_0, T_g), a_m(T_g, T_m), a_m(T_m, T_{d,0})$
Emissivity		$\epsilon$
Convection heat transfer		$h$

Table 4 : Full set of physical parameters required for the mesoscale thermal modelling

The determination of these mesoscale parameters will be in part made by considering the heat transfers on the macroscale of the composite plate. This macroscale modelling calls upon the 8 supplementary parameters listed in Table 5. Whereas some of them can be directly deduced from mesoscale parameters by means of a linear mixture rule accounting for the volume fractions of constituents (e.g. the volume density), for the others the meso-macro relations come from the equivalence of the RVE homogenized properties to the macroscale properties of the composite plate.

Physical property	Composite plate (macroscale)
Volume density	$\rho_{cp}$
Specific heat capacity	$c_{cp}(T)$
Thermal conductivity at $T_0$	$\lambda_{cp}^z(T_0), \lambda_{cp}^p(T_0)$
Coefficients of thermal conductivity variation	$\alpha_{cp}^z(T_0, T_g), \alpha_{cp}^z(T_g, T_m), \alpha_{cp}^z(T_m, T_{d,o})$ $\alpha_{cp}^p(T_0, T_{d,0})$

Table 5 : Parameters of the composite plate required for the macroscale thermal modelling

#### 4.2 Parameters determined from direct measurement techniques

As described in the introduction, each property (and its evolution with temperature) should ideally be determined separately from a dedicated experimental set-up. Due to technical constraints, only the following properties can be unequivocally determined from direct measurements:

##### Volume densities $\rho_{fb}$ and $\rho_m$

They are taken from the data of the composite supplier ( $\rho_{fb} = 1.76 \text{ g} \cdot \text{cm}^{-3}$  and  $\rho_m = 1.35 \text{ g} \cdot \text{cm}^{-3}$ ).

##### Emissivity

This property is set at 0.90, as commonly done for carbon-fiber reinforced laminates [31], and as set for the infrared thermography analyses (see Section 3.4).

##### Specific heat capacities $c_{cp}(T)$ , $c_{fb}(T)$ and $c_m(T)$

The experimental thermal changes of the matrix and composite specific heat capacities have been obtained from DSC analyses (see Section 3.1 for the description of the set-up). For technical restrictive reasons, analyses have been performed up to 300°C for the polymer matrix and 250°C for the composite material. Values have been extrapolated for higher temperatures. A linear mixture law has been used to deduce the fiber bundle heat capacity. All the results are presented in Figure 5. The measurements include both the sensible heat (required to raise the temperature of the material) and the enthalpy of matrix melting, as has been explained in [13]. The obtained values of these ‘‘apparent’’ heat capacities are taken as is to represent the specific heat capacities of each constituent in the simulations.

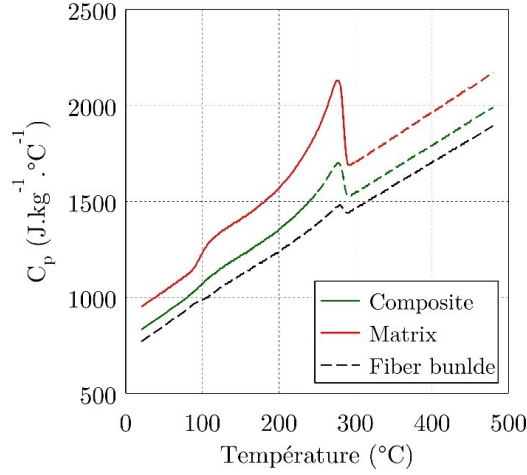


Figure 5 : Evolution of the specific heat capacities of the composite and of its constituents [13] according to temperature (continuous lines: exp. values from DSC; dashed lines: computed values)

### Thermal conductivities $\lambda_m(T_0)$ and $\lambda_{cp}^z(T_0)$

The values of thermal conductivities measured with the hot guarded plate method (cf. Section 3.3) at the ambient temperature are given in Table 6.

Parameter	$\lambda_{cp}^z(T_0)$	$\lambda_m(T_0)$
Average value [W. m <sup>-1</sup> .K <sup>-1</sup> ]	0.492	0.241
Standard deviation [W. m <sup>-1</sup> .K <sup>-1</sup> ]	0.006	0.005

Table 6 : Thermal conductivities measured with the hot guarded plate method

### 4.3 Thermal parameters identification

According to the preliminary statements on thermal parameters and having the results of direct measurements as explained in Sections 4.1 and 4.2, and as listed in Table 7, there remains 10 parameters to be determined at mesoscale, as well as the convection heat transfer coefficient  $h$  at macroscale.

	Known parameters	Unknown parameters	Identification step
	$\varepsilon, \rho_{cp}$	$h$	
Macroscale	$c_{cp}(T)$	$a_{cp}^z(T_0, T_g), a_{cp}^z(T_g, T_m), a_{cp}^z(T_m, T_{d,o})$	1
	$\lambda_{cp}^z(T_0)$	$\lambda_{cp}^p(T_0), a_{cp}^p(T_0, T_{d,0})$	
		$\lambda_{fb}^{ax}(T_0), a_{fb}^{ax}(T_0, T_{d,o})$	2
Mesoscale	$\rho_m, \rho_{fb}$	$\lambda_{fb}^r(T_0)$	3
	$c_m(T), c_{fb}(T)$	$a_m(T_0, T_g), a_m(T_g, T_m), a_m(T_m, T_{d,0})$	4
	$\lambda_m(T_0)$	$a_{fb}^r(T_0, T_g), a_{fb}^r(T_g, T_m), a_{fb}^r(T_m, T_{d,o})$	

Table 7 : List of known and unknown thermal parameters before the identification

Given the numerous possibilities of compensation effects, a large number of solutions of parameter sets could be obtained to reproduce the reference temperature measurements on the back and front face of the experimentally tested specimens. In order to limit as much as possible this number of potentially valid parameter sets and to construct an unambiguous and physically reliable model, a physics-driven methodology is constructed. It is based on the successive use of the macroscale modelling to which pertain reference temperature measures at the front and back face, and of the RVE mesoscale modelling. This methodology is divided into 4 steps (see Table 7) described in details in Appendix A. The identification is performed for an incident heat flux of 30 kW/m<sup>2</sup>. The resulting parameters are reported in Table 8. They have led to the temperature fields presented on Figure 7, to be compared to the experimental fields at three characteristic instants of the heat exposure. These identified values will be further discussed in Section 4.4.

	Parameter	Identified value	
Convective heat transfer	$h$	2.7 W.m <sup>-2</sup> .K <sup>-1</sup>	
Thermal conductivity	Composite plate	$\lambda_{cp}^z(T_0)$	0.492 W. m <sup>-1</sup> .K <sup>-1</sup>
		$\lambda_{cp}^p(T_0)$	10.5 W. m <sup>-1</sup> .K <sup>-1</sup>
	Matrix	$\lambda_m(T_0)$	0.241 W. m <sup>-1</sup> .K <sup>-1</sup>
		Fiber bundle	$\lambda_{fb}^{ax}(T_0)$
	$\lambda_{fb}^r(T_0)$		1.11 W. m <sup>-1</sup> .K <sup>-1</sup>
	Coefficients of thermal conductivity variation	Composite plate	$a_{cp}^z(T_0, T_{d,0})$
$a_{cp}^p(T_0, T_{d,0})$			-3.2 x 10 <sup>-4</sup> W.m <sup>-1</sup> .K <sup>-2</sup>
Matrix		$a_m(T_0, T_g)$	9.9 x 10 <sup>-4</sup> W.m <sup>-1</sup> .K <sup>-2</sup>
		$a_m(T_g, T_m)$	-1.3 x 10 <sup>-3</sup> W.m <sup>-1</sup> .K <sup>-2</sup>
		$a_m(T_m, T_{d,0})$	-2.2 x 10 <sup>-4</sup> W.m <sup>-1</sup> .K <sup>-2</sup>
		$a_{fb}^{ax}(T_0, T_{d,0})$	0.114 W.m <sup>-1</sup> .K <sup>-2</sup>
Fiber bundle		$a_{fb}^r(T_0, T_g)$	0.00087 W.m <sup>-1</sup> .K <sup>-2</sup>
		$a_{fb}^r(T_g, T_m)$	-0.0019 W.m <sup>-1</sup> .K <sup>-2</sup>
		$a_{fb}^r(T_m, T_{d,0})$	-0.016 W.m <sup>-1</sup> .K <sup>-2</sup>

Table 8: Final set of parameters for the thermal meso-scale model

The quality of the identification is evaluated from a quantitative point of view by computing the average difference in temperature over all the comparison points. This average and the associated standard deviation are given in Table 9 for three different incident heat flux: 30 kW/m<sup>2</sup> (one of the identification configurations), 40

and  $50 \text{ kW}\cdot\text{m}^{-2}$  as supplementary cases to examine the quality of the identification. The very small difference between, the simulation and the experimental value of the front face temperature (as compared to the differences on the back side) can be linked to the high weight  $w$  associated to this point in the calculation of the cost function  $F(P)$ :  $w=30$  versus  $w=1$  for the other points.

Incident heat flux ( $\text{kW}/\text{m}^2$ )	Front face error ( $^{\circ}\text{C}$ )	Back face error ( $^{\circ}\text{C}$ )
30	1	$20 \pm 8$
40	7	$22 \pm 8$
50	6	$23 \pm 8$

Table 9: Difference between experimental and simulated temperatures at the end of the step 1 identification process (on the macroscale composite plate), for the three considered incident heat fluxes. This difference is averaged through time, during the full history of heat flux exposure. On the back face, it is given in terms of an average over the 30 comparison points and of the standard deviation.

The identified parameters (cf. Table 8) have led to the time-evolution curves of temperature presented on Figure 8a. The identified set of parameters is further tested for incident heat fluxes of 40 and  $50 \text{ kW}/\text{m}^2$ , as presented on Figure 8b. For these higher heat fluxes, the experiments had been stopped when the front face temperature reached the temperature of matrix decomposition onset. Above that temperature, the measure of temperature from the thermocouples is no longer reliable because of the mechanisms of swelling and pyrolysis gas emission.

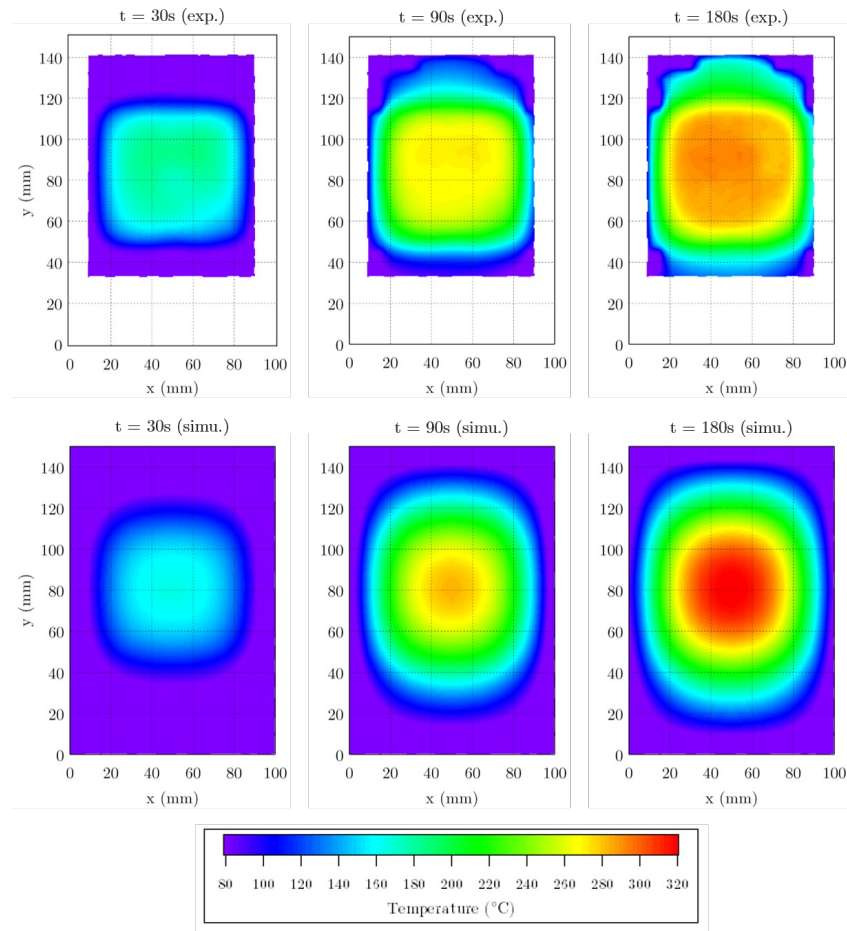


Figure 7: Experimental and simulated temperature fields on the back face of the plate at three different instants of heat exposure with an incident heat flux of 30 kW/m<sup>2</sup>. Simulations are conducted within the first step of the identification process and correspond on this figure to the final set of parameters

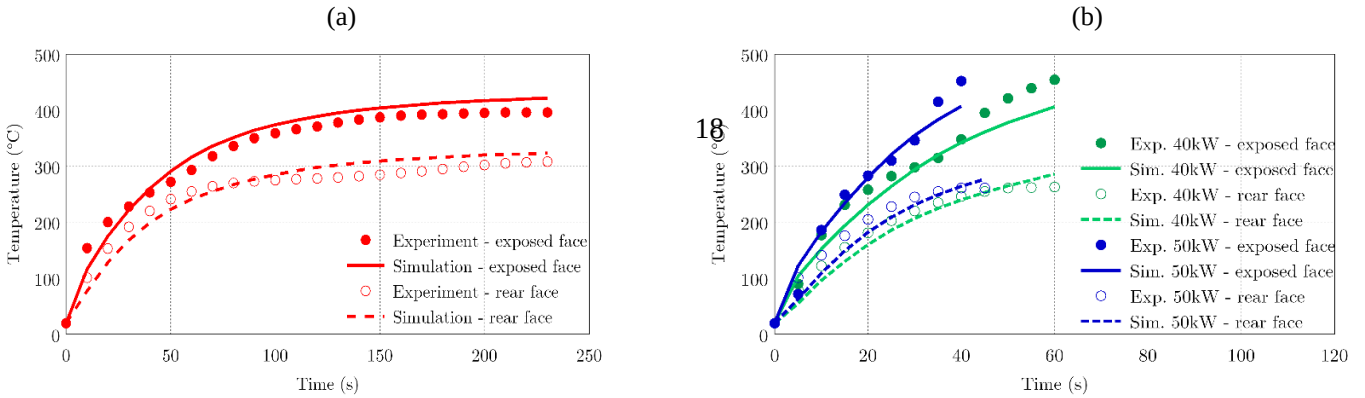


Figure 8: Temperature evolutions at the centers of back and front faces as measured experimentally and as simulated from the final set of identified parameters (reported in Table 8). (a) Case of the incident heat flux used in the identification process: 30 kW/m<sup>2</sup> - (b) Extension to incident heat fluxes of 40 and 50 kW/m<sup>2</sup>

For the incident heat fluxes of 30 and 40 kW/m<sup>2</sup>, one can note that simulations underestimate the temperature on the first part of the experiment and then overestimate this temperature. For a 50 kW/m<sup>2</sup> heat flux, the inverse effect is observed. These under- and over-estimations are correlated with the inflection points of the experimental curves, which are consequences of the matrix melting. The simulation fails at representing these inflection points. This could be due to the way the transition in heat capacity is represented in the modelling: it corresponds to a sharp transition at the given temperature  $T_m$  whereas DSC analyses show that it takes place progressively within a range of temperature. Besides, the way the enthalpy of melting is accounted for in the modelling (by representing its effect on the measured heat energy consumption, i.e. being included in the parameter used for the specific heat capacity) could be the object of analyses to improve the representation of the temperature evolution around the inflection point. Overall, the trends in the time-evolution of temperatures are correctly reproduced by simulation and the maximum difference between simulation and experiments remains lower than 10%.

#### 4.4 Discussion on thermal parameters identification

The identified thermal parameters result from a sequential process progressing from the macro-scale modelling of the composite plate to the meso-scale modelling on the RVE. Each step relies on the preceding one such that the reliability of the final parameters greatly depends on the quality of the identification at each step. Confidence may however be found from the richness of the reference data used for the identification: comparisons are made at different points of temperature measurement on the heat-exposed plate and on the full range of temperature evolution from the ambient to the temperature of matrix decomposition onset.

The value of  $h$  is compared with other values used in the literature for the analyses of heat transfers through a plate of composite or polymer material exposed to fire. With an inverse method, Cain and Lattimer have identified a value varying between 8 and 12 W.m<sup>-2</sup>.K<sup>-1</sup> [60] on the back face of a vertical plate. Other studies found simulations of heat transfer to well match experimental results with convective coefficients on the back

face of both horizontal and vertical plates of the order of  $5 \text{ W.m}^{-2}.\text{K}^{-1}$  [61-62]. The value identified in the present study ( $2.7 \text{ W.m}^{-2}.\text{K}^{-1}$ ) is of the same order of magnitude as in other studies. A decrease by a factor 2 with respect *e.g.* to the value obtained in Li et al [63] is consistent with the respective orientations of the outward normal to the back face: horizontal in our study, vertical and upward in [63]. Variations from a study to the other might also be related to the interactions of the back-face transfers with the mid-range environment, typically for example the anti-buckling fixture used in our study (see [17] for details), which limits *a priori* the convective flows.

Concerning  $\lambda_{fb}^r(T_0)$ , the relevance of its identified value can be verified indirectly by considering the upper and lower bounds of the composite plate conductivity  $\lambda_{cp}^z(T_0)$  computed from the linear and inverse mixture rules.  $\lambda_{cp}^z(T_0)$  is indeed determined only from  $\lambda_{fb}^r(T_0)$  and  $\lambda_m(T_0)$ , which itself is determined unequivocally from a direct measurement. Taking the identified value of  $\lambda_{fb}^r(T_0)$ , the related upper and lower bounds of  $\lambda_{cp}^z(T_0)$  are  $0.40$  and  $0.68 \text{ W.m}^{-1}.\text{K}^{-1}$ . The directly measured value of  $\lambda_{cp}^z(T_0)$  ( $0.492 \text{ W.m}^{-1}.\text{K}^{-1}$ ) effectively lies in between these bounds. The fact that it is closer to the lower than to the upper bound is related to the meso-structure: through the thickness, heat is transferred alternatively in a fiber bundle and in the matrix, which corresponds more to a serial model of heat conduction (lower bound) than to a parallel model (upper bound).

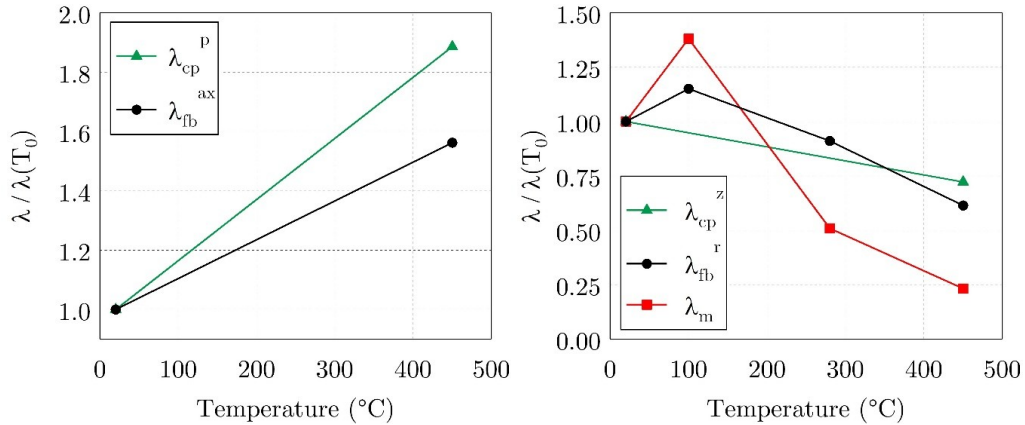


Figure 9: Evolution through temperature of normalized thermal conductivities after identification

As seen from Figure 9, because of the identification process, the conductivities of the constituents follow different evolutions upon heating:

1. An increase of the axial conductivity of fiber bundles; from the qualitative point of view, it is consistent with the measurements made in [64] on lignin-based microscale carbon fibers. This increase results in an increase of the in-plane composite plate. This observation is in line with the fact that fiber bundles represent a fully connected phase from side to side of the plate and that they have a much larger conductivity than the matrix.
2. A first increase up to  $T_g$  then a decrease to  $T_{d,0}$  for the radial fiber bundle conductivity. Very few experimental analyses allow to confirm or rebut this peculiar evolution since measurement of radial heat transfers at the small scale of an elementary carbon fiber requires specifically designed techniques, *e.g.* as proposed in Wang et al [64]. Their observations of small non-monotonous evolutions from 77K

to the ambient temperature suggest that an increase on a range of temperature from the ambient to 120°C is plausible.

3. As for the radial component of a fiber bundle, the conductivity of the matrix first increases to  $T_g$  and then decreases, which can be related with the change in the polymer structure at the transition temperature: vibrations of the atoms about their equilibrium position explains the increase up to  $T_g$  and after the transition, the increase in specific volume of the polymer -or in the space between atoms- would explain the reduction of the conductivity [50].

Finally, concerning the value of  $\lambda_{cp}^z(T)$ , one may expect it to lie in between those of  $\lambda_m(T)$  and  $\lambda_{fb}^r(T)$  on the full range of temperatures, such as any micro-macro scale transition scheme would produce. Precisely, the obtained  $\lambda_{cp}^z(T)$  does not result from the homogenization of meso-scale properties but was determined at an intermediate step of the identification process and its evolution is directly related to the choice which were then made to have a single ramp of variation on the full range of temperature, for sake of simplification. Making the choice of an evolution which is differentiated from an interval of temperature to the other, we then confirm that  $\lambda_{cp}^z(T)$  remains within the expected intervals defined by of  $\lambda_m(T)$  and  $\lambda_{fb}^r(T)$ , whatever  $T$  [64].

## 5 Thermo-mechanical modelling

### 5.1 Identification of mesoscale mechanical properties

#### 5.1.1 Preliminary assumptions on temperature dependences

As was explained in section 2.3 and 2.6, the considered mechanical behavior corresponds to moderate mechanical loads and is thereby restricted to the elastic linear behavior of the composite. Subsequently, as viscosity of the matrix is known not to play any role on the linear elastic response of the composite, the matrix itself is treated as a linear elastic material. Being an isotropic material, its behavior is exclusively defined by its Young's modulus and its Poisson's ratio. Assuming that the Poisson's ratio does not depend on temperature and taking the value  $\nu_m=0.36$  taken from the experimental analyses in [65], the only parameter to be identified concerning the elasticity of the matrix is the Young's modulus  $E_m(T)$  on the full range of investigated temperature.

Concerning its thermal dilation, interest is rarely paid in the literature on its evolution according to temperature, but only for the ambient temperature its value significantly depends on the actually used PPS. This has led us to set a constant thermal dilation which value is provided by the supplier:  $\alpha_m(T)=52 \times 10^{-6} K^{-1}$ . This assumption also finds its justification from the objectives of the study: to construct a comprehensive meso-structure-based methodology for the modelling of composite plate thermo-mechanics in the presence of severe out-of-plane thermal gradients. A concurrent objective is the identification of the involved physical mechanisms and of their respective contributions to the studied phenomena. Assumptions are then necessary to maintain a reasonable level of complexity, which settles a favorable ground for efficient realizations of simulation analyses. The same motivation has led to another simplification on temperature sensitivities: in the fiber bundle, both the elasticity and the thermal dilation are considered to have negligible dependencies to temperature. The

identification of the properties of each constituent of the RVE is the subject of the following sections, for the fiber bundles and the matrix respectively.

### 5.1.2 Fiber bundle

As stated in section 2.3, a fiber bundle is considered as a homogeneous isotropic transverse material with an orientation given by that of the fibers within the meso-structure. As classically done in meso-structure-based analyses, a fiber bundle can be assimilated to a composite ply with unidirectional fibers. The equivalence is made by setting the same volume fraction of matrix in the fiber bundle as that of the unidirectional composite. Given the volume fraction of matrix within the fiber bundle (17%) and the respective elasticity parameters of the matrix and of the elementary fibers, the model of Chamis [66] enables to compute the moduli of the isotropic transverse elasticity for the fiber bundle. Input and output values of the Chamis model are provided in Table 10. The constitutive laws of the model are defined in Equation 13, where the subscripts “L” and “T” refer respectively to longitudinal and transverse properties of the fiber bundle (fb):

$$\begin{aligned}
 E_{fb}^L &= V_f \cdot E_f^L + V_m \cdot E_m^\square & E_{fb}^{T21} &= \frac{E_m}{1 - \sqrt{V_f} \left( 1 - \frac{E_m}{E_f^T} \right)} \\
 G_{fb}^\square &= \frac{G_m}{1 - \sqrt{V_f} \left( 1 - \frac{G_m}{G_f^\square} \right)} & G_{fb}^{TL} &= \frac{G_m}{1 - \sqrt{V_f} \left( 1 - \frac{G_m}{G_f^{TL}} \right)} \\
 \nu_{fb}^\square &= V_f \cdot \nu_f^\square + V_m \cdot \nu_m^\square & \nu_{fb}^{TL} &= \frac{E_T}{2G_{fb}^{TL}} - 1
 \end{aligned} \tag{13}$$

Property	Matrix	Fiber	Fiber bundle
$E_m$ (GPa)	2.6		
$\nu_m$	0.36		
$E^L$ (GPa)		231	193
$E^T$ (GPa)		28.0	15.0
$G^\square$ (GPa)		24.0	11.7
$G^{TL}$ (GPa)		10.7	7.5
$\nu^\square$		0.26	0.28
$\nu^{TL}$		0.30	0.02

Table 8 : Input and output elasticity parameters of the Chamis model: Matrix [65], elementary fiber [58] and fiber bundle [59]

One can note that given the Chamis closed-form expressions of the fiber bundle elastic parameters according to those of an elementary fiber and of the matrix, any temperature dependence can easily be introduced on the mechanical properties of the fiber bundle. Concerning its thermal dilation coefficient, it is assumed to be described by a linear mixture rule of the fiber and matrix thermal dilation coefficients. In the axial direction, measurements provided in [59] show that the dilation coefficient varies within the range  $[-0.6, -0.2] \times 10^{-6} \text{ K}^{-1}$  for temperatures up to 450 °C and for different heat treatments of PAN-based fibers. As this value greatly

depends on the actual type of carbon fiber and since it remains negligible as compared to that of the matrix, it is set at 0. Concerning the radial dilation of a carbon fiber, as noticed in [59], fibers can display radial thermal contraction at the early stages of heat irradiation whereas the matrix expands. But once again the coefficient for the elementary fibers is supposed to be negligible and set at 0. Overall, these assumptions lead to an isotropic thermal dilation coefficient of the fiber bundle which is equal to 17% that of the matrix.

### 5.1.3 Polymer matrix

Bending tests conducted in the Dynamical Mechanical Analyses of the polymer matrix (cf. section 3.2) have enabled to extract the storage modulus in the range of temperatures  $[T_0, 200^\circ C]$ . Larger temperatures could not be tested because of technical restrictions on the experimental set-up. For the range of temperatures  $[200^\circ C, 300^\circ C]$ , we rely on the model proposed by Mahieux *et al.* [67], which, on the same basis of DMA provides an explicit expression of the Young's modulus evolution according to temperature ( $E_m(T)$ ), up to the polymer melting. This model accounts for the failure mechanisms occurring at each stage of the degradation of the polymer to describe the consequences of the phase transitions on the polymer stiffness: failure of electrostatic bonds at the glass transition temperature and failure of secondary bonds at the melting temperature. This enables to describe the phenomenology in terms of additive Weibull terms [68], as expressed in Eq. 14:

$$E_m(T) = (E_g - E_{rub}) \cdot \exp\left[-\left(\frac{T}{T_g}\right)^{m_g}\right] + E_{rub} \cdot \exp\left[-\left(\frac{T}{T_m}\right)^{m_m}\right] \quad (14)$$

$E_g$  and  $E_{rub}$  are the characteristic moduli of the polymer matrix in its glassy and rubbery states respectively.  $m_g$  and  $m_m$  are the Weibull parameters describing the kinetics of modulus transition at the glass transition and at the melting of the polymer.

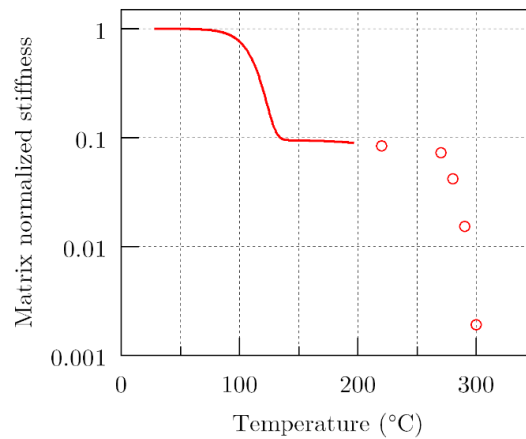


Figure 10: Evolution of the polymer matrix Young's modulus according to temperature in the range  $[T_0, 300^\circ C]$ . The continuous line refers to both DMA results and Mahieux model. Dots represent predictions from the Mahieux model in the range of unavailable DMA results

The set of parameters  $(E_g, E_{rub}, m_g)$  has been identified in the range of available DMA data  $[T_0, 200^\circ C]$  by minimizing the distance between the reference experimental curve and the Mahieux model. The value of the

Weibull parameter  $m_m$  is set equal to that identified by Mahieux for PPS. Figure 10 presents the resulting evolution of the Young's modulus according to temperature. This modulus is normalized by its value at ambient temperature. The continuous line corresponds to both the DMA results and the Mahieux model; the dots represent the extrapolation of the DMA curve according to the Mahieux model. All the parameters are resumed in Table 11.

$E_g$ (GPa)	$E_{rub}$ (GPa)	$T_g$ ( $^{\circ}C$ )	$T_m$ ( $^{\circ}C$ )	$m_g$	$m_m$
2.62	0.25	114	283	32	16

Table 9 : Parameters of the Mahieux model identified for the polymer matrix

## 5.2 Analysis under isothermal conditions

The temperature evolution of the composite plate macroscale longitudinal stiffness has been characterized by means of isothermal tensile tests conducted with the experimental set-up presented in section 3.5. Six different temperatures in the range  $[T_0, 320^{\circ}C]$  have been considered. They have been chosen such as to be representative of the different stages of polymer transition: at the ambient, close to the glass transition, in-between glass and melting transitions, just before and after melting. These isothermal tensile tests have been reproduced with FE simulations on the RVE, accounting for the full set of thermal and mechanical parameters identified for the studied composite material. Boundary conditions on the RVE correspond to a simple tensile test with imposed longitudinal displacements (along direction 1 on Figure 11a). In order to remove rigid body motions and to respect the periodicity of the laminate meso-structure, two of the lateral faces -with normals along directions 2 and 3- are set to remain inside their initial plane whereas the two others are only constrained to remain plane and parallel to their initial position. The RVE is then macroscopically free to deform in the transverse direction, as in simple tension.

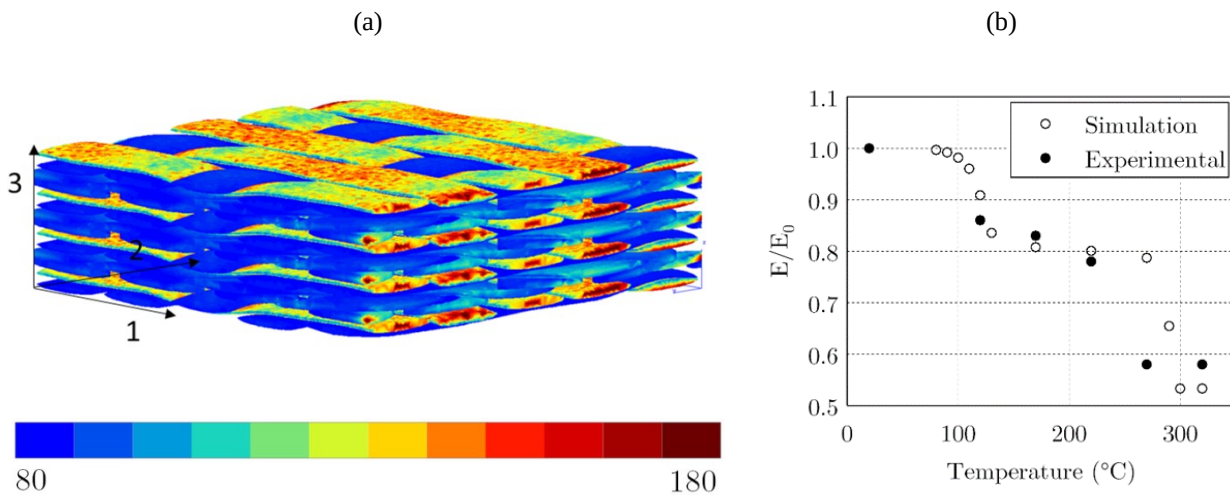


Figure 11: Simulations of isothermal strain-imposed tensile tests on the RVE at different temperatures. (a) Representation of the longitudinal stress field at given strain and 320°C - (b) Temperature evolution of the RVE apparent stiffness as compared to the experimental macroscale longitudinal stiffness of the composite plate. The stiffness is normalized by its value at ambient temperature.

Figure 11a illustrates the longitudinal stress field  $\sigma_{11}(T)$  obtained with an imposed longitudinal strain  $\varepsilon_{11}^{imp}$  at  $T=320^\circ C$ . For the sake of visualization, only the fiber bundles are represented. A strong heterogeneity in the stress field is observed, both inside fiber bundles and from a bundle to another one, depending primarily on its orientation with respect to the applied load but also on its location inside the RVE. In accordance with the definition of the RVE, the effective (macroscale) longitudinal stiffness of the composite plate is equal to the apparent stiffness of the RVE, which is obtained from the volume average of the longitudinal stress field over the volume  $V$  of the RVE as expressed in Eq. 15:

$$E_{cp}^L(T) = \frac{1}{V} \frac{\int_V \sigma_{11}(T) dV}{\varepsilon_{11}^{imp}} \quad (15)$$

To a first approximation, in order to estimate the validity of the model, the predicted value of  $E_{cp}^L$  at room temperature (46.1 GPa) is compared to the experimental value obtained on the same laminate (42.0 GPa [66]). The relative difference of about 10% between the two values can be related to the uncertainties of the constitutive elements' properties or the simplifying assumptions of the model. The evolution of  $E_{cp}^L$  according to temperature is shown in Figure 11b and compared to values from tensile tests conducted under isothermal conditions by means of a tube furnace [15].

One can note the very good quality of the prediction up to  $220^\circ C$ , i.e. from the ambient to the mid-run rubbery stage. Between 220 and  $270^\circ C$ , a significant drop is observed, in tight relation with matrix melting. Whereas the amount of the decrease obtained by modelling is similar<sup>24</sup> to that experimentally observed, the temperature at which this drop happens is not the same. This difference is presumably related to the hypothesis of a sharp melting process in the modelling: as indicated by DSC analyses, melting actually takes place progressively between  $220^\circ C$  and  $295^\circ C$ ; this is due to the mechanism of crystallite lamellae destruction, which strongly depends on the size of these lamellae and which subsequently occurs on a large temperature span.

Once the temperature of  $300^\circ C$  is reached (beyond which the stiffness of the matrix is supposed to remain constant), the matrix is in its molten state and the stiffness of the composite plate stabilizes at 52% its initial value against 58% experimentally. The thermomechanical model therefore slightly overestimates the stiffness in the ultimate stage of the matrix degradation. This can be related to the value attributed to the matrix Young's modulus in its molten state. The influence of this modulus on the computed composite plate stiffness can be analyzed from Figure 12. A proportional relation between the plate stiffness and the logarithm of the matrix stiffness is observed as the matrix stiffness decreases to 1% its ambient temperature value, which corresponds approximately to the fully molten state of the polymer. Below this value, i.e. for the fuzzy solid state between melting and decomposition, where it becomes delicate to describe the constitutive behavior of the matrix as that of a cohesive continuous medium, the relation progressively transforms into another logarithmic relation. This transition from a relation to the other highlights the complexity of the role of the matrix on the composite elasticity as the melting stage is reached for low values. From the quantitative point of view, one may estimate the importance of the value given to the matrix stiffness in its melting state: taken as 0.2% or 0.002% its ambient temperature value, a reduction of 47% or 52% of the composite plate stiffness is obtained respectively (Figure 12). This means that the predictions from the thermomechanical model should be considered with caution for temperatures corresponding to matrix melting: the high uncertainty pertaining to the experimental identification

of the matrix stiffness at such high temperatures might be the source of uncertainty on the composite macroscale, yet the value of the matrix stiffness is very low.

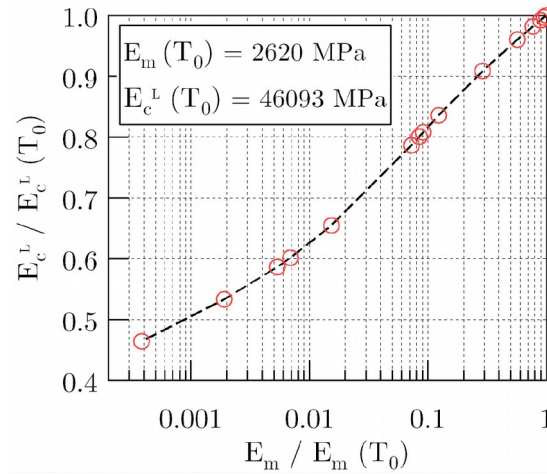


Figure 12: Evolution of the composite plate stiffness according to the polymer matrix Young's modulus. The respective moduli are normalized by their ambient temperature value  $E_m(T_0)$  and  $E_{cp}^L(T_0)$

### 5.3 Application to heat flux irradiation

This section is devoted to the application of the constructed model in the case of interest of this study: a mechanical load combined to a heat flux irradiating one face of the composite plate. In the present form, only stress distributions and stiffness reduction are simulated as a function of the temperature. In a forthcoming work, a failure analysis will be considered in the numerical model. The configuration of study is similar to that the one used at the step 4 of the thermal properties' identification process: the simulation is conducted on the RVE, accounting for the full thermal history of heating up with a heat flux of 20 Kw/m<sup>2</sup>, up to the stabilization of front and back face temperatures. In order to address one of the critical situations of a composite plate in its in-service conditions of a turbo-reactor nacelle, a constant tensile stress  $\sigma_{11} = 60 \text{ MPa}$  is applied during the heat flux exposure. The purpose of this simulation is to investigate the variations in the longitudinal stiffness of each ply of the laminates as temperature increases and to examine the concurrent efforts take up between the plies and their fiber bundles during the polymer matrix degradation. The evolution of the mean temperature in each ply of the laminate is shown in Figure 13a. The glass transition temperature of the matrix as well as the temperature of 270°C (start of the transition from the rubbery state to the molten state of the polymer matrix) are indicated, as they correspond to the onsets of the drops in stiffness of the composite plate associated to the matrix thermal degradation. The apparent (volume average) longitudinal stiffness of each ply is calculated as a function of time (Figure 13b) according to the expression given in Eq. 14, where V then refers to the volume of the ply. The glass transition temperature is reached within 13s on the front face and then, with a delay of only 7s, on the back face. Simultaneously a first sharp, rapid and quasi-instantaneous reduction in the longitudinal stiffness of all the plies occurs. The drop for 0/90° plies corresponds to 12% their initial value, whereas it is of 37% for ±45° plies, which is approximately the same as the one experimentally estimated in [65]: 33%.

(a)

(b)

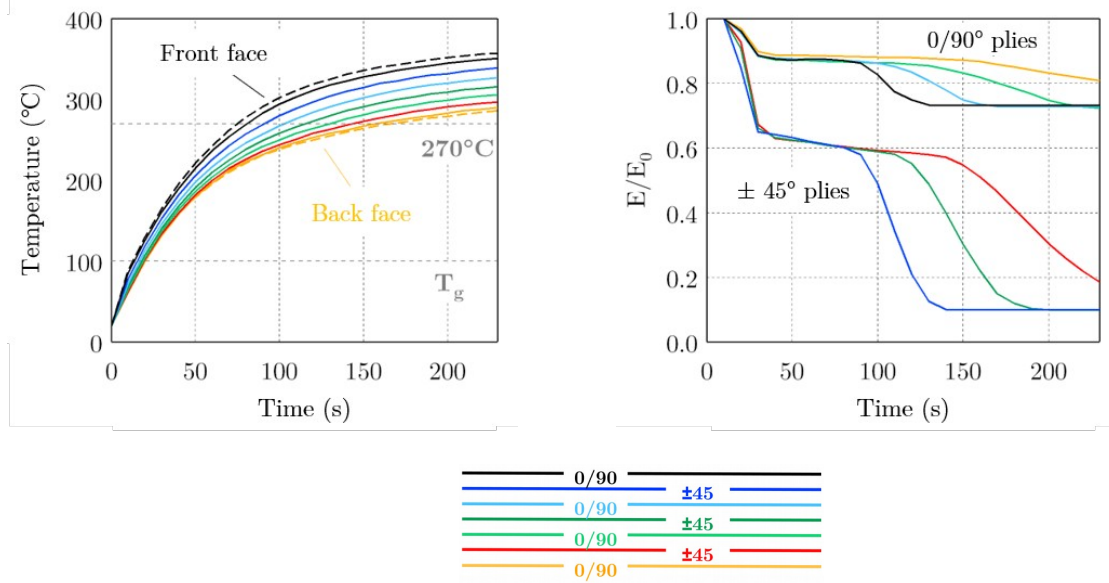


Figure 13: Analysis of the thermomechanical response of each ply within the laminate irradiated at  $20 \text{ kW/m}^2$  on one face and simultaneously exerting a constant tensile stress of  $60 \text{ MPa}$ . (a) Time-evolution of the temperature within each ply. (b) Time-evolution of the normalized longitudinal stiffness of each ply.

The second sequence of drops is spanned over the period of times at which the respective plies reach the matrix melting temperature. Once again, the plies at  $\pm 45^\circ$  undergo the largest reduction in stiffness: their residual stiffness is 10% their initial value, compared to 73% in  $0/90^\circ$  plies. This phenomenon is conform to the observations on the tight relationship between creep properties and the orientations of the plies in a laminate: given the properties of fibers and polymer matrix, creep elongation can only be due to the viscosity of the polymer matrix; laminates made from a stacking of  $\pm 45^\circ$  plies are precisely those exhibiting the largest creep elongations as compared to other stacking sequences, i.e. those having the largest sensitivity to the matrix properties, as presently observed.

The time-evolution of the longitudinal macro-scale strain of the composite during the creep test is presented in Figure 14a. The initial strain  $\varepsilon_{11}^0$  resulting from the mechanical loading has been subtracted from the total strain  $\varepsilon_{11}$  in order to focus only on the strain caused by the progressive matrix thermal degradation. There are 3 stages:

- The first increase corresponds to the period during which the matrix glass transition gradually settles throughout the plies.
- Once the glass transition temperature is reached all over the RVE and as long as the matrix melting temperature  $T_m$  is not reached, the variation of the matrix stiffness according to temperature remains small and consequently the strain remains virtually constant.
- As soon as  $T_m$  is reached in the exposed ply, the matrix stiffness undergoes a second drop and, in coordination with the continuous heating up over the successive plies, a second strain increase sequence occurs until the temperature exceeds the melting temperature at any point of the RVE. Above that temperature and up to the onset of matrix decomposition  $T_{d,0}$ , the change in matrix stiffness is

negligible and as a consequence the strain stabilizes when the temperature within the laminates is higher than 300°C.

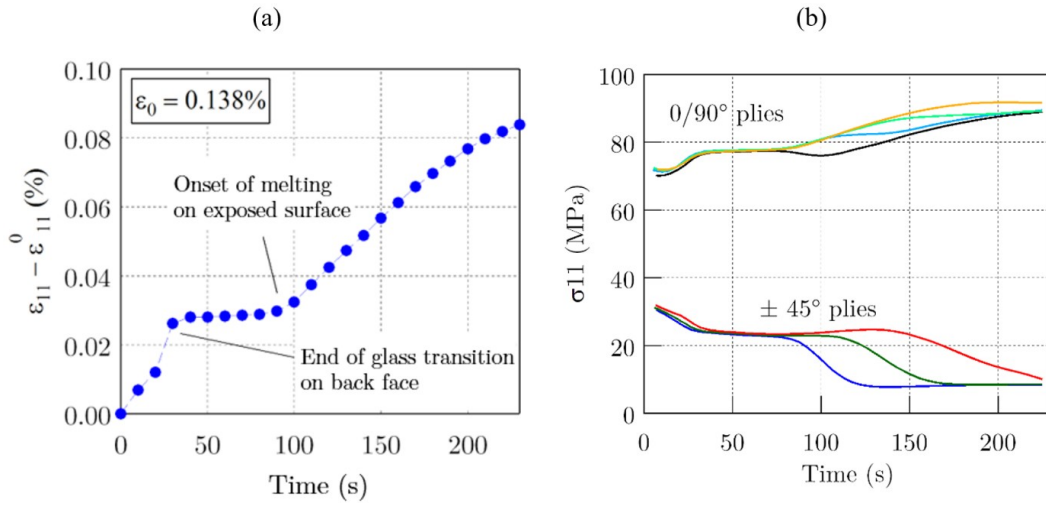


Figure 14: Thermo-mechanical response of the composite plate and of its different plies during a tensile creep test under a 20 kW/m<sup>2</sup> heat flux (anisothermal temperature conditions): (a) Evolution of the macro-scale longitudinal strain, (b) Evolution of the longitudinal stress within each ply

Figure 14b presents the time-evolution of the apparent longitudinal stress within each ply during the creep test. As for the macro-scale strain, an alternation of variation and stabilization regimes is observed. They are separated by characteristic times corresponding to the occurrence of either the matrix glass transition or its melting. These characteristic times are delayed in accordance to the distance of the considered ply with respect to the exposed face. A clear concordance between stress decrease regimes in  $\pm 45^\circ$  plies and stress increase regimes in  $0/90^\circ$  plies can also be detected: as the stress declines within a  $\pm 45^\circ$  ply, because of the high sensitivity of their stiffness to temperature, the stress is transferred to  $0/90^\circ$  plies and consistently increases. The respective contributions of the  $0/90^\circ$  plies to take up the load transferred from  $\pm 45^\circ$  plies is greatly dependent on their position with respect to the heat flux. One may note for example that, in the exposed ply, the stress decreases slightly at  $t=80$  s because of its stiffness degradation, and then increases again because of the transfer of the load from the underneath  $\pm 45^\circ$  ply. The consequences of matrix thermal degradation and ultimately melting -up to the onset of its degradation- on stress and strain redistributions within the laminate can also be analyzed on the local scale of a ply.

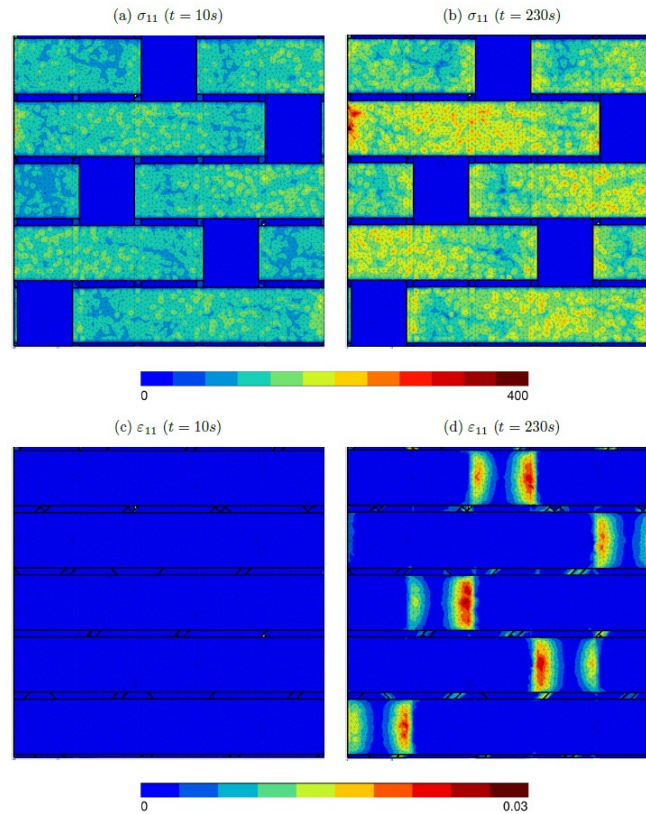


Figure 15: Views on the longitudinal stress (a,b) and strain fields (c,d) on the front face ( $0/90^\circ$  ply) of laminates exposed to a heat flux ( $20 \text{ kW/m}^2$ ) under constant tensile stress ( $60 \text{ MPa}$ , horizontal). The left column (a,c) corresponds to the instant  $t=10s$ , where the matrix glass transition temperature has not yet been reached and the right column (b,d) corresponds to  $t=230s$ , where the matrix is fully melted

Figure 15 provides the longitudinal stress and strain fields on the exposed face of the laminate, at two characteristic instants: at the early stage of the combined heat flux and creep test, before the matrix glass transition is reached and at the final stage of the test, where a temperature of  $350^\circ\text{C}$  is reached on the exposed face (cf. Figure 13a), which corresponds to a fully molten state for the matrix. One can note the increase through time of the longitudinal stress in the  $0^\circ$ -oriented fiber bundles, which results from the melting of the matrix and the concomitant reduction in stiffness of the underneath  $\pm 45^\circ$ . This simulation also allows to highlight the influence of the weave on the localization of the longitudinal strains: as the matrix melts, a significant increase in longitudinal strain is observed in crimp regions, i.e. in the areas where warp fibers overlap with weft fibers.

## 6 Conclusions

A meso-macro numerical modelling is proposed to simulate the thermo-mechanical behavior of thermoplastic-based composite laminates subjected to a mechanical loading under transient anisothermal conditions. The effects of a one-side fire exposure on the degradation of the laminate's mechanical properties is simulated. The adopted meso-scale approach consists in (i) representing explicitly each constituent of the laminate -matrix and fiber bundles- within a representative volume element, (ii) to assign them the appropriate temperature-dependent properties, and (iii) to have the boundary-value problem of combined mechanical loading and fire exposure solved by the finite element method under the hypothesis of a weak coupling between thermal transfers and mechanics.

The first difficulty is to identify the temperature-dependent thermal and mechanical properties which govern the constitutive behavior of the constituents over the considered range of temperatures, from the ambient to the onset of the polymer matrix decomposition. A methodology is thus proposed to identify, first, the undetermined thermal parameters for a C/PPS quasi-isotropic laminate. It is based on a step-by-step process involving macro-scale simulations on a composite plate and meso-scale ones on the representative volume element. The parameters are identified by comparing front and back face temperature fields to experimentally measured ones, for a heat flux of 30 kW/m<sup>2</sup>. The quality of the identification is discussed with respect to theoretical bounds provided by mixture laws and validated by considering the supplementary cases of thermal transfers (heat fluxes of 40 and 50 kW/m<sup>2</sup>).

The second difficulty concerns the identification of the mechanical properties of each constituent over the encountered temperature range. It includes the glass transition of the polymer matrix and its melting, which result in dramatic changes in its stiffness. The laminates' anisotropy is accounted for in the three dimensions of the meso-structured representative volume element: not only to make the distinction between the respective plies (0°/90° or ±45°) but also in the representation of the crimp regions of the weave. By comparison with the experimental results, the capability of the model to correctly predict the degradation of the longitudinal stiffness of the laminate up to matrix melting temperature is demonstrated. Finally, the model is tested to evaluate the consequences of a combined one-side heat flux and longitudinal tension at a constant stress in the laminate. Though it shows some limitations, the present model provides a solid basis for developing a more predictive model over a wide temperature range, and to account for different types of combined loadings.

From the presented meso-macro approach, a database of thermal and mechanical parameters was built over a temperature range up to the thermal decomposition temperature. Hopefully, this work will capture the attention of the industrial and scientific community to inspire new developments for larger structural application analysis.

## References

- [1] A.P. Mouritz, A.G. Gibson. Fire properties of polymer composite materials. N° 143 Solid mechanics and its applications. Springer, Dordrecht, 2006.
- [2] U. Sorathia, C.M. Rollhauser, W. Allen Hughes. Improved fire safety of composites for naval applications. *Fire and Materials* 1992; 16(3).
- [3] K. Grigoriou, A.P. Mouritz. Influence of ply stacking pattern on the structural properties of quasi-isotropic carbon-epoxy laminates in fire. *Composites Part A* 2017; 99: 113-120.
- [4] T. Bhat, E. Kandare, A.G. Gibson, P. Di Modica, A.P. Mouritz. Tensile properties of plant fibre-polymer composites in fire. *Fire and Materials* 2017; 41(8).
- [5] A.P. Mouritz, Z. Mathys. Mechanical properties of fire-damaged glass-reinforced phenolic composites. *Fire and Materials* 2000; 24(2).
- [6] S-G. Hong, S-Y. Chang. Fire performance and mechanical properties of acrylonitrile-butadiene-styrene copolymer/modified expandable graphite composites. *Fire and Materials* 2011, 6(4).
- [7] Z. Yu, A. Zhou. Effect of flame heat flux on thermal response and fire properties of char-forming composite materials. *Fire and Materials* 2012; 38(1).
- [8] T.N.A. Browne. A model for the structural integrity of composite laminates in fire. PhD doctoral dissertation, University of Newcastle upon Tyne, 2006.
- [9] A.G. Gibson, M.E.O. Torres, T.N.A. Browne, S. Feih, A.P. Mouritz. High temperature and fire behaviour of continuous glass fibre/polypropylene laminates. *Composites Part A* 2010; 41(9): 1219–1231.
- [10] S. Feih, A.P. Mouritz. Tensile properties of carbon fibres and carbon fibre polymer composites in fire. *Compos Part A* 2012; 43: 765-772.
- [11] F. Lacroix, V. Allheily, K. Diener, A. Eichhorn, M. Gillet, G. L'Hostis. Thermomechanical behavior of aeronautic structural carbon epoxy composite submitted to a laser irradiation. *Composite Structures* 2016; 143: 220-229.

- [12] S. Timme, V. Trappe, M. Korzen, B. Schartel. Fire stability of carbon fiber reinforced polymer shells on the intermediate-scale. *Composite Structures* 2017; 178: 320–329.
- [13] Y. Carpier, B. Vieille, N. Delpouve, E. Dargent. Isothermal and anisothermal decomposition of carbon fibres polyphenylene sulfide composites for fire behavior analysis. *Fire Safety Journal* 2019; 109: 102868.
- [14] Y. Carpier, B. Vieille, A. Coppalle, F. Barbe. About the tensile mechanical behaviour of carbon fibers fabrics reinforced TP composites under very high temperature conditions. *Composites Part B* 2020; 181: 107586.
- [15] J.A. Milke, A.J. Vizzini. The effects of simulated fire exposure on glass-reinforced thermoplastic materials. *Journal of Fire Protection and Engineering* 1993; 5(3), 113-124.
- [16] Y. Carpier, B. Vieille, A. Coppalle, F. Barbe. Study of thermomechanical coupling in carbon fibers woven-ply reinforced TP laminates: Tensile behavior under radiant heat flux. *Polymer Comp.* 2020; 41: 3552– 3563.
- [17] Y. Carpier, B. Vieille, M.A. Maaroufi, A. Coppalle, F. Barbe. Mechanical behavior of carbon fibers PPS composites exposed to radiant heat flux and constant compressive force. *Comp Structures* 2018; 200: 1-11.
- [18] B. Vieille, A. Coppalle, C. Keller, M.-R. Garda, Q. Viel, E. Dargent. Correlation between post fire behavior and microstructure degradation of aeronautical polymer composites. *Materials and Design* 2015; 74:76–85.
- [19] A. G. Gibson, M. E. O. Torres, T. N. A. Browne, S. Feih, A. P. Mouritz. High temperature and fire behaviour of continuous glass fibre/polypropylene laminates. *Composites Part A* 2010; 41(9): 1219–1231.
- [20] W. Zhang, B. Gu, B. Sun. Thermal-mechanical coupling modelling of 3D braided composite under impact compression loading and high temperature field. *Composites Science and Technology* 2017; 140 : 73-88.
- [21] S. Shi, J. Liang, G. Lin, G. Fang. High temperature thermomechanical behavior of silica-phenolic composite exposed to heat flux environments. *Composites Science and Technology* 2013; 87: 204-209.
- [22] G. Lubineau, P. Ladevèze, D. Violeau. Durability of CFRP laminates under thermomechanical loading: A micro–meso damage model. *Composites Science and Technology* 2006; 66(7–8): 983-992.
- [23] P. Upadhyaya, S. Singh, S. Roy. A mechanism-based multi-scale model for predicting thermo-oxidative degradation in high temperature polymer matrix composites. *Comp Sc. and Technology* 2011; 71(10): 1309-1315.
- [24] J.K. Farooqi, M.A. Sheikh. Finite element modelling of thermal transport in ceramic matrix composites. *Computational Materials Science* 2006; 37(3): 361-373.
- [25] J. Aboudi, S.M. Arnold, B.A. Bednarczyk. Fully Coupled Thermomechanical Analysis of Multiphase Composites. In: *Micromechanics of Composite Materials*. Editor(s): Jacob Aboudi, Steven M. Arnold, Brett A. Bednarczyk, Butterworth-Heinemann, 2013, Pages 541-576.
- [26] G. Chatzigeorgiou, N. Charalambakis, Y. Chemisky, F. Meraghni. Periodic homogenization for fully coupled thermomechanical modeling of dissipative generalized standard materials, *International Journal of Plasticity*, Volume 81, 2016, Pages 18-39.
- [27] E. Tikarouchine, G. Chatzigeorgiou, Y. Chemisky, F. Meraghni. Fully coupled thermo-viscoplastic analysis of composite structures by means of multi-scale three-dimensional finite element computations, *International Journal of Solids and Structures*, Volume 164, 2019, Pages 120-140.
- [28] A.P. Mouritz, S. Feih, E. Kandare, Z. Mathys, A.G. Gibson, P.E.D. Jardin. Review of fire structural modelling of polymer composites. *Compos Part A* 2009; 40: 1800-1814.
- [29] S. Feih, Z. Mathys, A.G. Gibson, A.P. Mouritz. Modelling the compression strength of polymer laminates in fire. *Composites Part A* 2007; 38(11): 2354–2365.
- [30] S. Feih, Z. Mathys, A.G. Gibson, A.P. Mouritz. Modelling the tension and compression strengths of polymer laminates in fire. *Compos Sci Technol* 2007; 67: 551-564.
- [31] G.A. Pering, P.V. Farrell, G. S. Springer, Degradation of Tensile and Shear Properties of Composite Exposed to Fire or High Temperature. *Journal of Composite Materials* 1980; 14: 54-68.
- [32] J.K. Chen, C.T. Sun, C.I. Chang. Failure Analysis of a Graphite/Epoxy Laminate Subjected to Combined Thermal and Mechanical Loading. *Journal of Composite Materials* 1980; 19(5): 408-423.
- [33] C.A. Griffis, J.A. Nemes, F.R. Stonesifer, C.I. Chang. Degradation in Strength of Laminated Composites Subjected to Intense Heating and Mechanical Loading. *Journal of Composite Materials* 1981; 20(3): 216-235.
- [34] A.G. Gibson, Y-S. Wu, H.W. Chandler, J.A.D. Wilcox: A model for the thermal performance of thick composite laminates in hydrocarbon fires. *Revue de l'Institut Français du Pétrole* 1995; 50(1): 69–74.
- [35] E. Kandare, G.J. Griffin, S. Feih, A.G. Gibson, B.Y. Lattimer, A.P. Mouritz. Fire structural modelling of fibre–polymer laminates protected with an intumescent coating. *Composites Part A* 2012; 43(5): 793-802.
- [36] J. Zhuge, J. Gou, R-H. Chen, J. Kapat. Finite element modeling of post-fire flexural modulus of fiber reinforced polymer composites under constant heat flux. *Composites Part A* 2012, 43(4): 665-674.
- [37] S.E. Boyd, J.V. Bausano, S.W. Case, J.J. Lesko. Mechanistic approach to structural fire modeling of composites. *Fire Technol* 2009; 47: 941-983.
- [38] S.E. Boyd, J.J. Lesko, S.W. Case. Compression creep rupture behavior of a glass/vinyl ester composite laminate subject to fire loading conditions. *Compos Sci Technol* 2007; 67: 3187-3195.
- [39] Boyd SE, Case SW, Lesko JJ. Compression creep rupture behavior of a glass/vinyl ester composite subject to isothermal and one-sided heat flux conditions. *Compos Part A* 2007; 38:1462-1472.

- [40] S.E. Boyd, S.W. Case, J.J. Lesko. Composite life under sustained compression and one sided simulated fire exposure: characterization and prediction. *Compos Part A* 2006; 37: 1092-1100.
- [41] D. Swanson, J. Wolfrum. Effects of simultaneous compression and one-sided heat flux on the time to failure of carbon fiber-reinforced polymer composites. *Journal of Composite Materials* 2018; 52(13): 1809-1819.
- [42] T. Bhat, E. Kandare, A.G. Gibson, P. Di Modica, A.P. Mouritz. Compressive softening and failure of basalt fibre composites in fire: Modelling and experimentation. *Composite Structures* 2017; 165: 15-24.
- [43] P.T. Summers, B.Y. Lattimer, S. Case, S. Feih. Sensitivity of thermo-structural model for composite laminates in fire. *Composites Part A* 2012; 43(5): 783-792.
- [44] C. Lautenberger, G. Rein, C. Fernandez-Pello. The application of a genetic algorithm to estimate material properties for fire modeling from bench-scale fire test data. *Fire Safety Journal* 2006; 41(3): 204-214.
- [45] M. Chaos, M. M. Khan, N. Krishnamoorthy, J.L. de Ris, S.B. Dorofeev. Evaluation of optimization schemes and determination of solid fuel properties for CFD fire models using bench-scale pyrolysis tests. *Proceedings of the Combustion Institute* 2011; 33(2): 2599-2606.
- [46] B.Y. Lattimer, J. Ouellette, J. Trelles. Measuring properties for material decomposition modeling. *Fire Materials* 2011; 35: 1-17.
- [47] Vieille B, Albouy W. Influence of matrix ductility on the high-temperature fatigue behaviour of notched and unnotched thermoplastic and thermoset laminates. *Journal of Reinforced Plastics and Composites*. 2015;34(21):1755-1764.
- [48] Blond D, Vieille B, Gomina M, Taleb L. Correlation between physical properties, microstructure and thermo-mechanical behavior of PPS-based composites processed by stamping. *Journal of Reinforced Plastics and Composites*. 2014;33(17):1656-1668.
- [49] W.A. Gray, R. Müller. *Engineering Calculations in Radiative Heat Transfer*. International Series on Materials Science and Technology. Edited by Elsevier, 1974.
- [50] W. Albouy, B. Vieille, L. Taleb. Experimental and numerical investigations on the time-dependent behavior of woven-ply PPS TP laminates at temperatures higher than Tg. *Compo Part A* 2013; 49: 165-178.
- [51] E-S. Shin, S. J. Kim. A predictive measure of thermomechanical coupling in elasto-viscoplastic composites. *Composites Science and Technology* 1999; 59(7): 1023-1031.
- [52] E. Ahci, R. Talreja. Characterization of viscoelasticity and damage in high temperature polymer matrix composites. *Composites Science and Technology* 2006; 66(14): 2506-2519.
- [54] A.C. Long, L.P. Brown. Modelling the geometry of textile reinforcements for composites: TexGen. In *Composite Reinforcements for Optimum Performance*, p. 239-264. Elsevier, 2011.
- [55] S. Daggumati. Concurrent modelling and experimental analysis of meso-scale strain fields and damage in woven composites under static and fatigue tensile loading. PhD thesis, Ghent University, 2011.
- [56] Z-set, Material and structure analysis suite, <http://www.zset-software.com>
- [57] Test standard EN 6035. Aerospace series - fiber-reinforced plastics - test method. Determination of notched and unnotched tensile strength. Published by the Europ. Association of aerospace industries. April 1996.
- [58] C. Pradere, J.C. Batsale, J.M. Goyh  n  che, R. Pailler, S. Dilhaire. Thermal properties of carbon fibers at very high temperature. *Carbon*, Volume 47, Issue 3, 2009, Pages 737-743.
- [59] C. Sauder, J. Lamon, R. Pailler. Thermomechanical properties of carbon fibres at high temperatures (up to 2000  C). *Composites Science and Technology* 2002; 62(4): 499-504.
- [60] C. Cain et B. Y. Lattimer. Measuring Properties for Material Decomposition Modeling. *Journal of ASTM International*, 7(1):1-26, 2009.
- [61] Goupil, A. C., Craveur, J. C., Mercier, B., & Barabinot, P. (2017). Decomposing composite material structures: Practical modelling issues for the large-scale fire tests. *Journal of Structural Fire Engineering*.
- [62] Li, J., Gong, J., & Stolarov, S. I. (2014). Gasification experiments for pyrolysis model parameterization and validation. *International Journal of Heat and Mass Transfer*, 77, 738-744.
- [63] K. Eiermann, K.-H. Hellwege. Thermal conductivity of high polymers from -180 C to 90 C. *Journal of Polymer Science* 1962; 57(165): 99-106.
- [64] R. Wang, H. Zobeiri, H. Lin, W. Qu, X. Bai, C. Deng, X. Wang (2019), Anisotropic thermal conductivities and structure in lignin-based microscale carbon fibers, *Carbon*, 147, 58-69.
- [65] J. Aucher. Etude comparative du comportement de composites   matrice thermoplastique ou thermodurcissable. PhD doctoral dissertation, INSA Rouen Normandie, 2009.
- [66] C.C. Chamis. Simplified composite micromechanics equations for hygral, thermal and mechanical properties, NASA, Technical memorandum, 1983.
- [67] C. A. Mahieux et K. L. Reifsnider. Property modeling across transition temperatures in polymers: application to thermoplastic systems. *Journal of Materials Science*, 37: 911-920, 2002.
- [68] C.A. Mahieux. A Systematic Stiffness-Temperature Model for Polymers and Applications to the Prediction of Composite Behavior. PhD doctoral dissertation, Virginia Tech, 1999.